Complex macroevolution of pterosaurs

Article *in* Current Biology · February 2023

DOI: 10.1016/j.cub.2023.01.007

CITATIONS
5

READS
653

3 authors:

Yilun Yu
Chinese Academy of Sciences
18 PUBLICATIONS **97** CITATIONS
SEE PROFILE

Chi Zhang
Chinese Academy of Sciences
23 PUBLICATIONS **3,158** CITATIONS
SEE PROFILE

Xing Xu
Chinese Academy of Sciences
366 PUBLICATIONS **14,624** CITATIONS
SEE PROFILE

Report

Current Biology

Complex macroevolution of pterosaurs

Highlights

- New datasets were analyzed to understand pterosaur diversification and evolution
- The analyses reveal a long flourishing period followed by a short waning period
- Multiple factors affect pterosaur macroevolution, but in different ways
- A Cretaceous biodiversity decline is probably present in large terrestrial amniotes

Authors

Yilun Yu, Chi Zhang, Xing Xu

Correspondence

zhangchi@ivpp.ac.cn (C.Z.), xu.xing@ivpp.ac.cn (X.X.)

In brief

Yu et al. estimate diversification and morphological rates and morphological disparity values in pterosaur evolution, which reveal an ~115-Ma flourishing period followed by an ~65-Ma waning period. This study suggests the presence of a biodiversity decline of large-sized terrestrial amniotes starting in the mid-Cretaceous.

Yu et al., 2023, Current Biology *33*, 1–10
February 27, 2023
https://doi.org/10.1016/j.cub.2023.01.007

CellPress

Please cite this article in press as: Yu et al., Complex macroevolution of pterosaurs, Current Biology (2023), https://doi.org/10.1016/j.cub.2023.01.007

Current Biology

CellPress

Report

Complex macroevolution of pterosaurs

Yilun Yu,[1,2] Chi Zhang,[1,3,*] and Xing Xu[4,5,6,*]
[1]Key Laboratory of Vertebrate Evolution and Human Origins, Institute of Vertebrate Paleontology and Paleoanthropology, Chinese Academy of Sciences, Beijing, China
[2]University of Chinese Academy of Sciences, Beijing, China
[3]Center for Excellence in Life and Paleoenvironment, Chinese Academy of Sciences, Beijing 100044, China
[4]Centre for Vertebrate Evolutionary Biology, Yunnan University, Kunming, China
[5]Shenyang Normal University, Paleontological Museum of Liaoning, Shenyang, China
[6]Lead contact
*Correspondence: zhangchi@ivpp.ac.cn (C.Z.), xu.xing@ivpp.ac.cn (X.X.)
https://doi.org/10.1016/j.cub.2023.01.007

SUMMARY

Pterosaurs, the earliest flying tetrapods, are the subject of some recent quantitative macroevolutionary analyses from different perspectives.[1–2] Here, we use an integrative approach involving newly assembled phylogenetic and body size datasets, net diversification rates, morphological rates, and morphological disparity to gain a holistic understanding of the pterosaur macroevolution. The first two parameters are important in quantitative analyses of macroevolution, but they have been rarely used in previous pterosaur studies.[1–12] Our study reveals an ~115-Ma period—from Early Triassic to Early Cretaceous—of multi-wave increasing net diversification rates and disparity, as well as high morphological rates, followed by an ~65-Ma period—from Early Cretaceous to the end of the Cretaceous—of mostly negative net diversification rates, decreasing disparity, and relatively low morphological rates in pterosaur evolution. Our study demonstrates the following: (1) body size plays an important role in pterosaur lineage diversification during nearly their whole evolutionary history, and the evolution of locomotion, trophic, and ornamental structures also plays a role in different periods; (2) birds, the other major flying tetrapod group at the time, might have affected pterosaur macroevolution for ~100 Ma; and (3) different mass extinction events might have affected pterosaur evolution differently. Particularly, the revealed decline in pterosaur biodiversity during the Middle and Late Cretaceous periods provides further support for the possible presence of a biodiversity decline of large-sized terrestrial amniotes starting in the mid-Cretaceous,[13,14] which may have been caused by multiple factors including a global land area decrease during these periods.

RESULTS

Pterosaur lineage diversification evolution

Generally, pterosaur biodiversity increased for most of their evolution from 245 to 125 Ma, as indicated by the positive net diversification rates in most time bins during this time interval. It then decreased from 125 Ma up until their extinction 66 Ma, as indicated by the negative rates in most time bins (Figures 1A, S2A, and S2E). During the general biodiversity increase from 245 to 125 Ma, there is a more detailed multiple-wave pattern: the first wave reaches its peak value at 225–215 Ma, the second wave at 195–185 Ma, the third wave at 175–165 Ma, and the fourth wave at 135–125 Ma. These increases are interrupted by three distinct biodiversity decreases that reach lows around 215–205, 185–175, and 155–145 Ma, respectively. During the general decrease in pterosaur diversity from 125 to 66 Ma, the diversification rates strongly fluctuate, with two large decreases (reaching lows at 125–115 and 85–75 Ma, respectively). The four intervening increases are all caused by relatively high speciation rates and low extinction rates, whereas the five decreases relate to high extinction rates and relatively low speciation rates (Figures 1B, 1C, S2B, S2C, S2F, and S2G).

Evolutionary rates of overall morphology

The morphological evolutionary rates are relatively high from the Triassic through to the earliest Cretaceous but relatively low during most of the Cretaceous (Figure 1D). There are four major increases of the rates: the first increase reaches a peak value at ~240 Ma, followed by a relatively quick decrease to a low value at ~228 Ma; the second increase reaches a peak value between ~197 and ~195 Ma, followed by a gradual decrease to a low value at ~153 Ma; the third increase at ~141 Ma followed a gradual decrease to a low value at ~113 Ma; and the final increase reached a peak value near to the end of the Cretaceous (Figure 1D). Partitioned analyses show that the evolutionary rates of different anatomical regions are extremely heterogeneous: the cranial skeleton region (CSR) evolved fast in the latest Triassic, much of the Jurassic, and particularly in the earliest Cretaceous (Figure 1E); the axial skeleton region (ASR) evolved fast in much of the Jurassic and Cretaceous (Figure 1F); the pectoral girdle and forelimb region (PFR) evolved fast in the Middle Triassic and much of the Jurassic (Figure 1G); and pelvis and hindlimb region (PHR) evolved particularly fast in the Late Triassic (Figure 1H). All four anatomical regions display relatively fluctuating rate changes from the Triassic through to the earliest Cretaceous

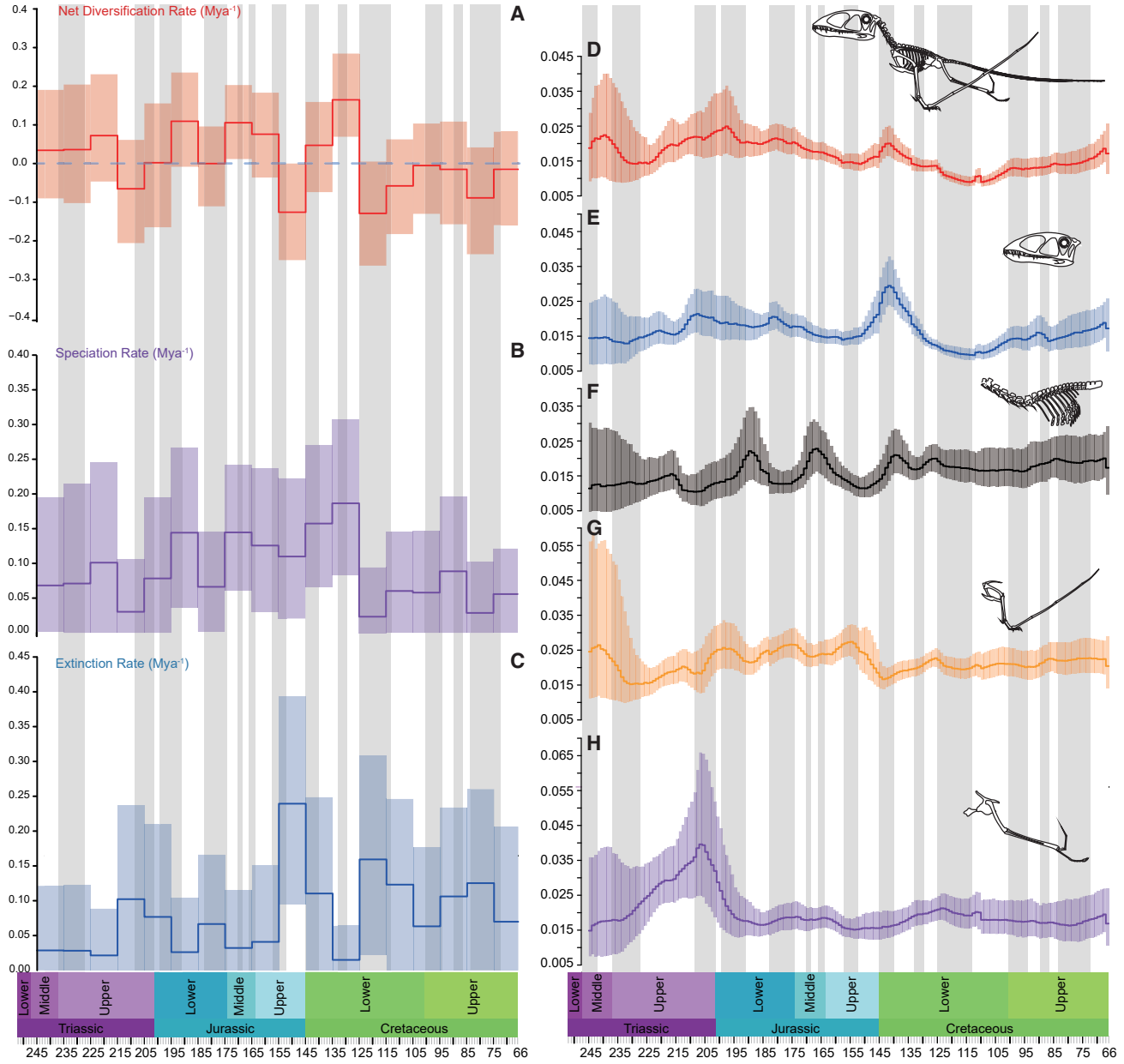

Figure 1. Pterosaur diversification and morphological evolutionary rate through time

(A–C) Net diversification (A), speciation (B), and extinction rate (C) through time, estimating from skyline fossilized birth-death (SFBD) model with CIS tree.
(D) Unpartitioned (D) morphological rate estimated from SFBD model with parsimony strict consensus tree (PSC).
(E–H) CSR (E), AXR (F), PFR (G), and PHR (H) rates estimated from SFBD model with PSC tree.
The colored boxes in (A)–(C) are 95% highest posterior density (HPD) intervals, and they represent upper and lower quartiles in (D)–(H). The skeleton reconstruction is modified from Witton.[15]
See also Figures S1–S3.

but relatively smooth ones thereafter until the end of the Cretaceous.

Across the pterosaur tree, evolutionary rates display an increasing trend along the branches from near the root of the tree up to the Ornithocheiroidea, although in earlier branches, the accelerated pattern is not as distinct as in later branches (Figure 2A). Pteranodontia and Archaeopterodactyloidea display accelerated evolution along the branches within the clades, but Anurognathidae and Azhdarchoidea show high rates along the branches leading to these two clades. The partitioned analyses have revealed different patterns in different anatomical regions (Figures 2B–2E). The evolutionary rates of the CSR are high along many branches across the tree, particularly along the late-diverging lineages (e.g., along the branch leading to the Tapejaromorpha and branches within this clade, as well as along branches within the Pteranodontia); a similar pattern is also

Please cite this article in press as: Yu et al., Complex macroevolution of pterosaurs, Current Biology (2023), https://doi.org/10.1016/j.cub.2023.01.007

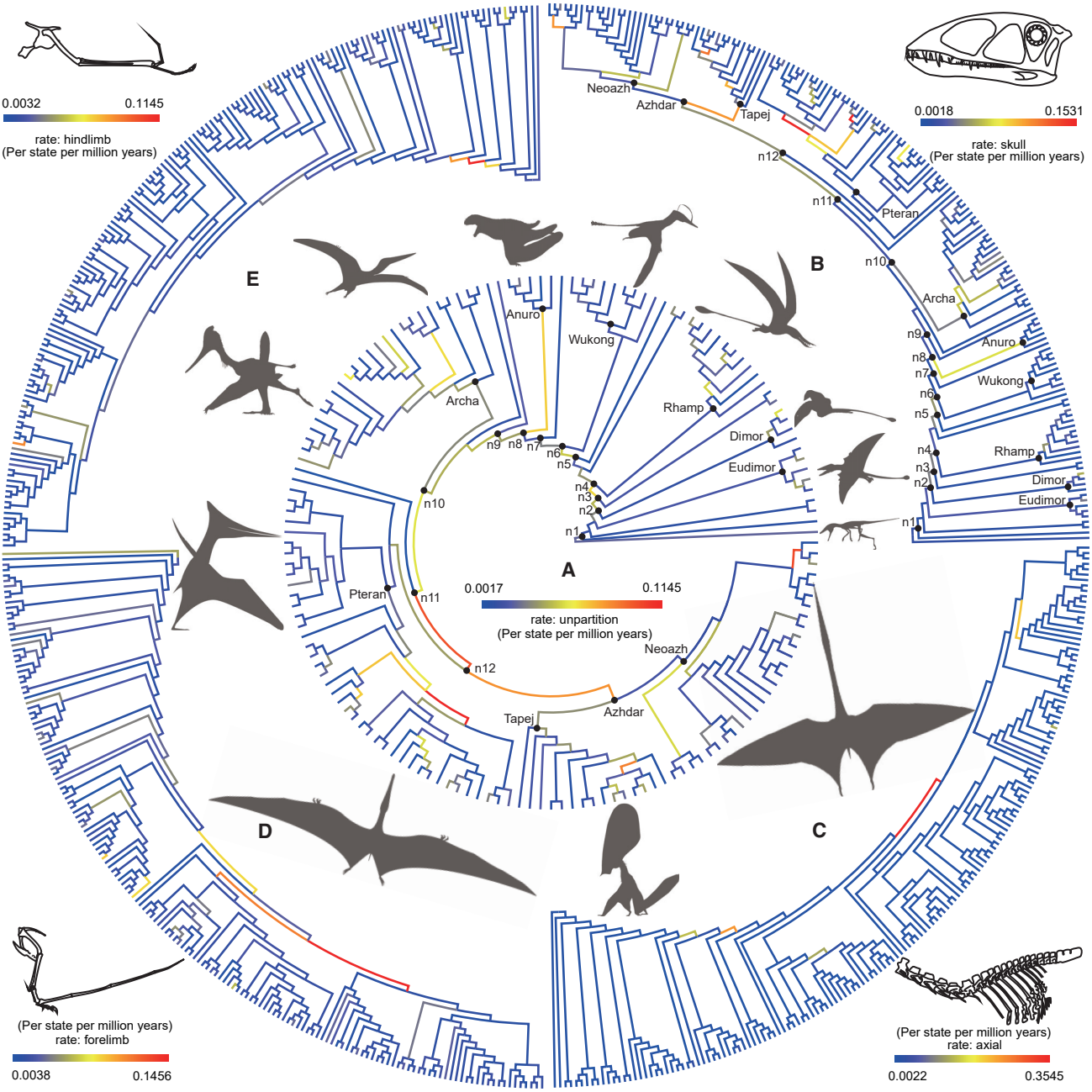

Figure 2. Morphological evolutionary rate mapping on phylogeny

(A) Unpartitioned morphological rate estimated from PSC tree.

(B–E) CSR (B), AXR (C), PFR (D), and PHR (E) rates estimated from partitioned model with PSC tree.

Abbreviations are as follows: n1, Pterosauria; n2, Macronychoptera; n3, Novialoidea; n4, Breviquartossa; n5, Pterodactylomorpha; n6, Monofenestrata; n7, Pterodactyliformes; n8, Caelicodracones; n9, Pterodactyloidea; n10, Lophocratia; n11, Eupterodactyloidea; n12, Ornithocheiroidea; Eudimor, Eudimorphodontoidea; Rhamp, Rhamphorhynchidae; Wukong, Wukongopteridae; Anuro, Anurognathidae; Archa, Archaeopterodactyloidea; Pteran, Pteranodontia; Azhdar, Azhdarchoidea; Tapej, Tapejaromorpha; and Neoazh, Neoazhdarchia. Silhouettes are from http://phylopic.org/, and skeleton reconstructions are from Witton.[15] See also Table S1.

seen in PFR evolution; the rates of PHR are high along some branches across the tree, and the highest rates are present along early-diverging lineages; and those of ASR are high along only a few branches, particularly at the branch leading to the Ornithocheiroidea.

Disparity changes of overall morphology

Morphological disparity values reach their first peak value at ~215 Ma, followed by a significant drop to the low value at ~200 Ma;[16] then achieve the second peak value at ~160 Ma, followed by a drop to the low value at ~140 Ma; and finally reach

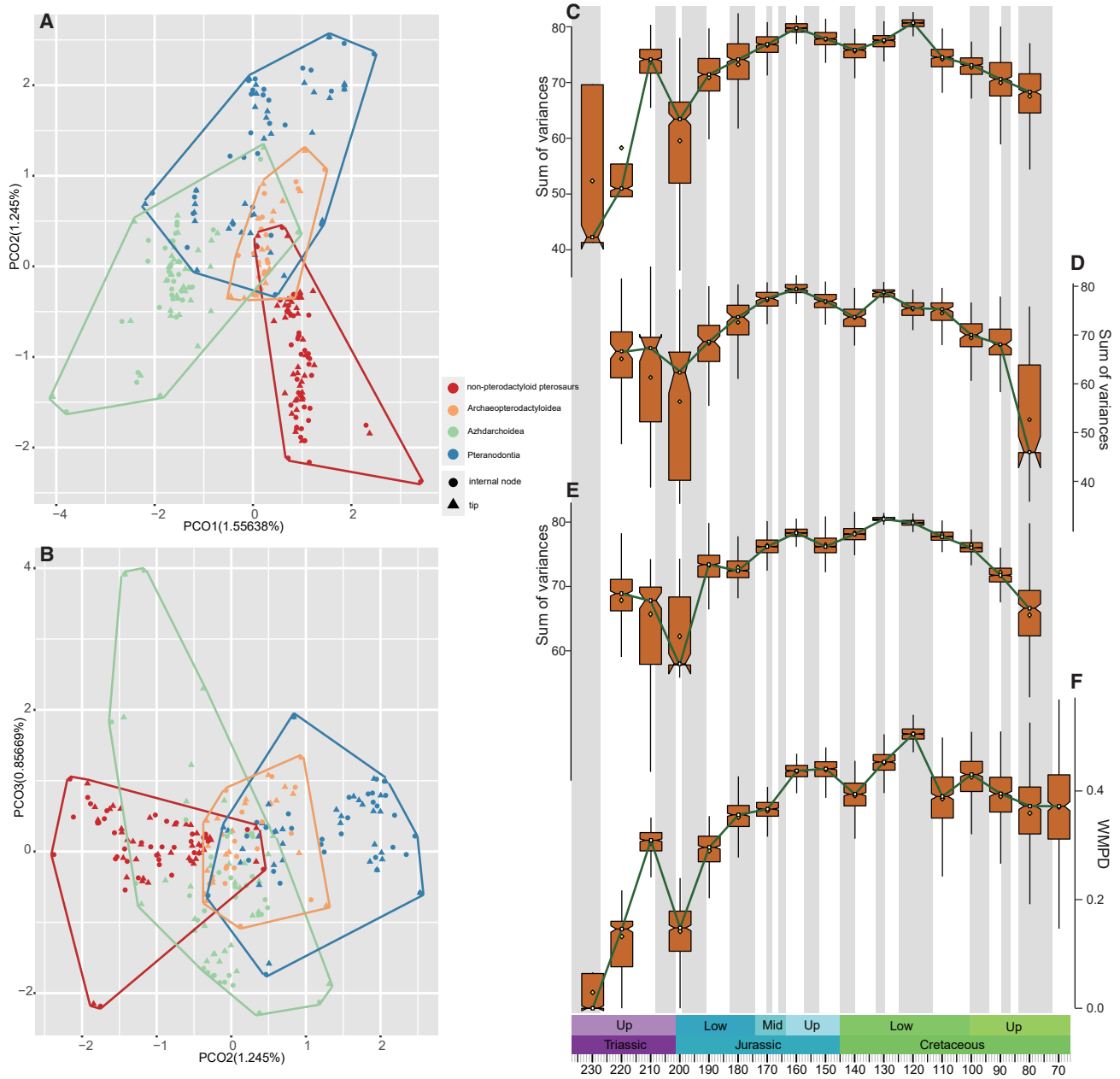

Figure 3. Morphological disparity through time with a phylomorphospace approach

Ancestral state reconstruction was performed on dated PSC tree. Only three axes were shown on the figure, but the axes that together comprise 90% of total variance (219 axes) were used for disparity summarizing and substantial statistical analyses.

(A and B) Phylomorphospace comparison of different groups of pterosaurs shown by PCO_1 and PCO_2 (A) and by PCO_2 and PCO_3 (B).

(C) Time-binned sum of variances.

(D) Sum of variances summarized with time-sliced method (equal split model) based on majority rule consensus tree.

(E) Medians of sum of variances summarized with time-sliced method (equal split model) based on 100 randomly sampled posterior tree.

(F) Time-binned weighted mean pairwise distance.

For (C)–(E), the sample size of the last bin/slice is very small, and the interval between upper and lower quartiles is very large, which is not shown in the figure. See also Figure S4 and Table S2.

the third peak at ~120 Ma, which is followed by a gradual decrease until the end of the Cretaceous (Figures 3C–3F). Comparatively, previous studies have revealed only the Cretaceous peak, which is probably due to the relatively small sample size in these analyses.[1,6–9] We tested the disparities obtained in each time bin (or point) with that preceding it, demonstrating a significant shift in disparity between neighboring time bins (points). Our correlation test demonstrates a strong correlation

between different anatomical regions in terms of morphological disparity change, which has been also revealed by a previous study,[10] although a statistical correlation does not necessarily arise from correlated evolution. Furthermore, our analyses indicate that the non-pterodactyloid pterosaurs occupied larger morphospace than the three major pterodactyloid clades (i.e., Archaeopterodactyloidea, Pteranodontia, and Azhdarchoidea) (Figures 3A, 3B, and S4; Table S2). In most analyses, Archaeopterodactyloidea has the lowest disparity among the four groups, and Pteranodontia has the highest disparity among the three pterodactyloid subgroups (Figures 3A, 3B, and S4; Table S2).

Body mass evolution

Evolutionary rates of body mass (data used in analyses and marginal likelihood used for model selection are given in Tables S3 and S4) are low along most pterosaur branches, except those leading to Anurognathidae, Ornithocheiroidea, and Quetzalcoatlinae, and several branches within Ctenochasmatidae and Azhdarchoidea, which are probably associated with gigantism and miniaturization (Figure 4A). Body mass through time analyses divide the pterosaur evolution into a small-sized period before 160 Ma and a large-sized period after 160 Ma. Body mass disparity analyses reveal a period of relatively low disparity values followed by a fluctuating period with relatively high disparity values (Figures 4B and 4C).

DISCUSSION

It should be noted that these results were produced based on trees with different sample sizes, different tree topologies, different timescaled trees, and under different model assumptions, and body mass macroevolutionary analyses were made using different data sources. Correlation tests demonstrate that geological sampling proxies were not correlated with our estimated diversification rates and disparity values (Figure S3; Table S2). Our statistical analyses, following the methods used in Upham et al.[17] and Pyron et al.[18] also suggest that the estimated morphological evolutionary rates have not been affected by missing data (Table S1). Consequently, our results are robust, and particularly, they are not heavily affected by the Signor-Lipps effect, which has been considered to have a major effect on the reconstruction of pterosaur evolution.

Our analyses produce significant results pertaining to important questions such as how speciation and extinction change during macroevolution and how different traits drive lineage diversification.[19] The first ~115-Ma period of pterosaur evolutionary history is characterized by mostly positive net diversification rates (here referred to as the flourishing period) and largely matches the speciation-rate curve (Figures 1A, 1B, and S2). The last ~65-Ma period of pterosaur evolutionary history is characterized by mostly negative net diversification rates (here referred to as the waning period) and is a collective result of relatively high extinction rates, low speciation rates, and the five distinct decreases in diversification rates corresponding to five distinct extinction-rate increases (Figures 1 and S2). This general diversification pattern is well explained by the results of our morphological evolution analyses. The initial flourishing period featured high morphological evolutionary rates and increasing disparity, whereas the later waning period was accompanied by low morphological evolutionary rates and a continuous decrease in disparity; though both lineage diversification and morphological evolutionary rates display a small increase in the latest Cretaceous.

During the initial flourishing period, the first lineage diversification increase in the mid-Late Triassic represents a radiation adapted to the aerial ecospace, which is supported by the high evolutionary rate of PFR in the Middle Triassic (Figure 1G). The increased disparity (Figures 3C–3F) and the geographically widely distributed and ecologically diverse early pterosaurs[20,21] provide further support for this radiation. The second and third increases of diversification rate in the mid-Early and Middle Jurassic, respectively, are associated with relatively high morphological evolutionary rates in all four body regions (CSR, ASR, PFR, and PHR) (Figures 1D–1H) and a continuous increase in disparity (Figures 3C–3F). These increases probably pertain to further locomotor system improvements,[5] feeding system innovations such as fish feeding and new food resources,[15,22,23] and new habitats.[24]

The fourth lineage diversification increase in the mid-Early Cretaceous is possibly linked to factors including new habitats associated with lakes, rivers, and coasts,[25] and/or new flying modes.[26] There is a distinct increase in the morphological evolutionary rate of the CSR in the earliest Cretaceous (Figure 1E), which results in a great diversity of cranial ornamentations and feeding apparatuses (e.g., herbivorous, durophagous, and omnivorous) among Early Cretaceous pterosaurs.[1,15,25,27] These diverse cranial ornamentations in pterosaurs might be linked with species recognition and/or sexual selection.[27–30]

Our analyses reveal that body mass disparity does not seem to be associated with diversification rate change in pterosaur evolution, but body mass itself seems to be associated with the latter. The flourishing period is mostly associated with small body size, although the earliest Cretaceous of the flourishing period featured large body size (Figures 4B and 4C). This exception can be explained by the occupation of new niches by relatively large pterosaurs[11,4] and by sexual selection and/or other recognition mechanisms among large-sized pterosaurs during the earliest Cretaceous. Although large body size might have played a role in the Early Cretaceous radiation, it is mostly associated with the waning period (Figures 4B and 4C) that features relatively high extinction rates (Figures 1C, S2C, and S2G).

Several extrinsic factors also might have affected pterosaur macroevolution. Previous studies suggest an interaction between birds and pterosaurs because they might have shared similar ecospace and food resources.[11,23,31–35] Our analyses reveal that there is a continuous decrease in net diversification (Figures 1A, S2A, and S2E) and a distinct decrease in morphological disparity (Figures 3C–3F) between 165 and 145 Ma in pterosaur evolution, contrary to a correspondent diversification and disparity increase in bird evolution.[36–38] This supports the hypothesis that early birds might have affected the evolution of small-sized pterosaurs during the Late Jurassic,[39,40] but admittedly, pygostylian birds, the potential competitors of small pterosaurs,[5] are absent in the fossil record of this period. The Early Cretaceous pterosaurs had a distinctly larger body size than contemporaneous birds (Figure 4) and thus presumably avoided direct competition with the latter. However, at least Late Cretaceous pterosaurs (e.g., some azhdarchoids[41]) might have had

Please cite this article in press as: Yu et al., Complex macroevolution of pterosaurs, Current Biology (2023), https://doi.org/10.1016/j.cub.2023.01.007

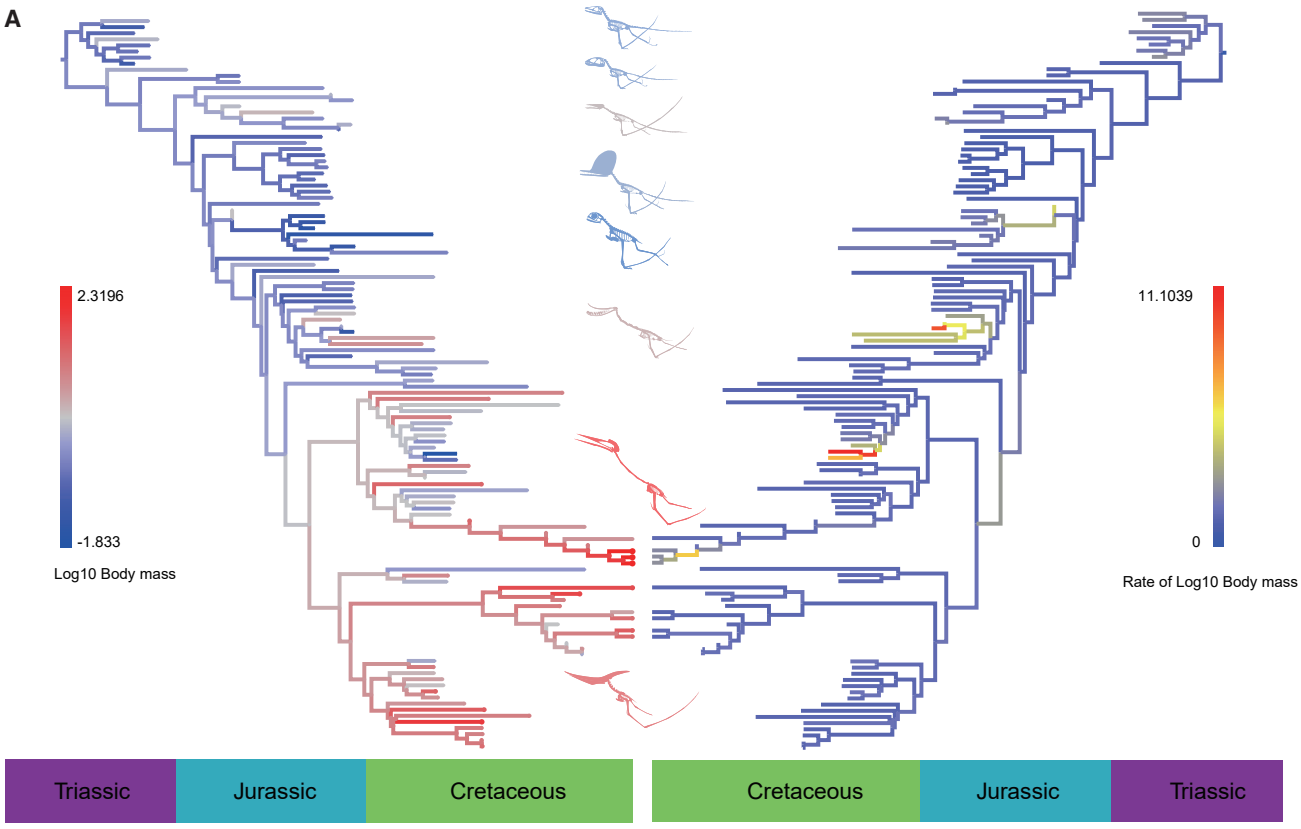

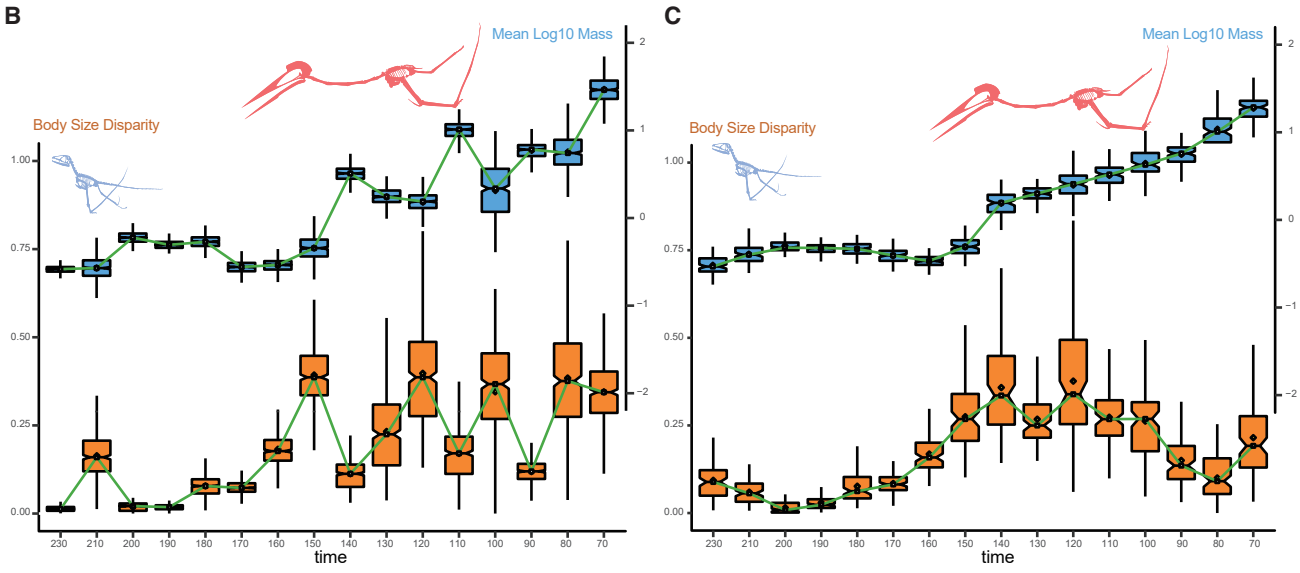

Figure 4. Patterns of body mass (log_{10} transformed) evolution

Using estimated body mass from Table S4 (and using dated CIS tree and Pagel's lambda as tree transformation).

(A) Mapping of body mass evolution rate and ancestral state on tree.

(B and C) Mean and disparity of body mass summarized with time-bin technique (B) and time-sliced method (equal split model) (C). The colored boxes represent upper and lower quartile in (B) and (C). The skeleton reconstruction is modified from Witton.[15]

See also Tables S3 and S4.

to face competition pressure from early birds because they were similar in body size to some Late Cretaceous birds.[11,42] The documented increasing disparity and diversification rate of Late Cretaceous birds[36,38] indicate that birds might have provided increasing competitive pressures for pterosaurs during this period.

Some mass extinction events such as the ones during the Middle Cretaceous and at the end of the Cretaceous also affected pterosaur biodiversity evolution,[43] as indicated by distinct decreases in net diversification from 125 to 115 and 85 to 75 Ma, respectively, and by the extinction of the clade at the end of the Cretaceous (Figures 1A, S2A, and S2E). Other mass extinction events, such as the ones near the end of the Triassic and in the Early Jurassic, led to no distinct decrease in net diversification (there is a distinct diversification rate decrease at ~215–205 Ma before the end-Triassic extinction event), although the disparity values display a significant drop around the end of the Triassic.

Previous studies have explored the temporal relationships between the increases in morphological evolutionary rate, disparity, and phylogenetic diversity/taxic diversity in different organismal groups, and they have identified several different patterns.[44] Most organismal groups show a pattern of morphological disparity earlier than phylogenetic diversity,[45] although some other patterns are also known.[46–52] Because phylogenetic diversity is a commonly used parameter for macroevolutionary studies in paleontology, we also reconstructed pterosaur phylogenetic diversity through time for comparative purposes (Figure S2I). Our analyses indicate that pterosaurs first increased the evolutionary rate, then the diversification rate, and finally phylogenetic diversity and morphological disparity. Pterosaurs are similar to early-diverging and lepidosaurian amniotes[47,48] in having a pattern of evolutionary rate earlier than morphological disparity and similar to North American carnivores,[53] Cenozoic ungulates,[46] and Mesozoic mammals[49] in having a pattern of phylogenetic diversity coupled with morphological disparity, but they are different from many other organismal groups in the temporal relationships of these major parameters. Finally, our analyses reveal that in pterosaur evolution, different anatomical regions display different morphological evolutionary rates but similar morphological disparity curves. These suggest that the decoupling of morphological rate evolution between different anatomical regions is not necessarily leading to a similar pattern of disparity evolution.

The decline of pterosaur biodiversity in the Middle and Late Cretaceous periods, which has been noticed by previous studies[6,7,12] and strongly supported by our analyses, deserves special mention. Some studies suggest that a decline in either diversification rate or phylogenetic diversity/taxic diversity is present in some other terrestrial clades during the Middle and Late Cretaceous periods, including most non-avialan dinosaur clades except hadrosauriforms and ceratopsians[13,54,55] (but see Bonsor et al.[56] for an opposing view), rhynchocephalians,[14] and probably some non-marine crocodyliforms such as notosuchians[57–59] (admittedly, a decline is not present in any well-preserved regional crocodyliform assemblages[60,61]). However, it has been hypothesized that this period was important for the diversification of many organismal groups and particularly for the origin of modern diversity, leading to the proposals of Cretaceous Terrestrial Revolution (KTR)[62,63] and Angiosperm Terrestrial Revolution (ATR).[64] Compared with the taxa rising in diversification during KTR/ATR,[63,64] the terrestrial animals that have been suggested to have declined in biodiversity are large in size. There are several possible external factors contributing to the decline of large-sized terrestrial amniotes, including land reduction,[65] climate changes,[66] and the Middle Cretaceous volcanic activities,[67] among others. The land reduction might have affected more significantly large-sized animals in biodiversity than the small animals because large body size has been demonstrated to be linked with a higher extinction risk,[68,69] and exponentially fewer niches are available for larger animals,[11,70] particularly when habitat size is smaller.[71] Admittedly, more data and analyses are needed to confirm the presence of biodiversity decline in most dinosaur clades and other comparatively large-sized terrestrial animal groups, as we did for pterosaur biodiversity evolution. It should be noted that several analyses indicate a high diversity for pterosaurs[4] and some other large-sized terrestrial animals[72,73] during the latest Cretaceous, suggesting that the biodiversity decline is restricted to the Middle Cretaceous. Nevertheless, the presence of both KTR/ATR and a possible Cretaceous biodiversity decline might be a reflection of terrestrial faunal change featured by a diversification of small-sized animals accompanied by a biodiversity decline in large-sized animals. This complex macroevolutionary history is recoverable using an integrative approach combining different lines of data and different methods.

STAR★METHODS

Detailed methods are provided in the online version of this paper and include the following:

- KEY RESOURCES TABLE
- RESOURCE AVAILABILITY
  - Lead contact
  - Materials availability
  - Data and code availability
- EXPERIMENTAL MODEL AND SUBJECT DETAILS
- METHOD DETAILS
  - Supertree assembly and data matrix construction
- QUANTIFICATION AND STATISTICAL ANALYSIS
  - Morphological and diversification rate analyses
  - Morphological disparity analyses
  - Correlation test with sampling proxies
  - Body mass estimation
  - Body mass macroevolutionary analyses

SUPPLEMENTAL INFORMATION

Supplemental information can be found online at https://doi.org/10.1016/j.cub.2023.01.007.

ACKNOWLEDGMENTS

We thank Christian Foth and two anonymous reviewers for critical and constructive comments, Michael Pittman for editing and commenting on the manuscript, Tanja Stadler for discussions on identifiability issues in the fossilized birth-death (FBD) model, Graeme T. Lloyd for helpful suggestion on disparity analyses, and Shunxing Jiang for discussions on pterosaur morphology and sharing reference. This work was supported by the National

Natural Science Foundation of China (42288201 and 41688103) and the International Partnership Program of Chinese Academy of Sciences (132311KYSB20180016) to X.X. and the Hundred Young Talents Program of Chinese Academy of Sciences (Y902061) and the Strategic Priority Research Program of Chinese Academy of Sciences (XDB26030300) to C.Z.

AUTHOR CONTRIBUTIONS

Y.Y., C.Z., and X.X. designed the project. Y.Y. collected the data and performed all the analyses. Y.Y., X.X., and C.Z. analyzed the results and wrote the manuscript.

DECLARATION OF INTERESTS

The authors declare no competing interests.

Received: September 2, 2022
Revised: November 13, 2022
Accepted: January 5, 2023
Published: February 13, 2023

REFERENCES

1. Zhou, C.F., Gao, K.Q., Yi, H., Xue, J., Li, Q., and Fox, R.C. (2017). Earliest filter-feeding pterosaur from the Jurassic of China and ecological evolution of Pterodactyloidea. R. Soc. Open Sci. *4*, 160672.
2. Slack, K.E., Jones, C.M., Ando, T., Harrison, G.L., Fordyce, R.E., Arnason, U., and Penny, D. (2006). Early penguin fossils, plus mitochondrial genomes, calibrate avian evolution. Mol. Biol. Evol. *23*, 1144–1155.
3. Dean, C.D., Mannion, P.D., and Butler, R.J. (2016). Preservational bias controls the fossil record of pterosaurs. Palaeontology *59*, 225–247.
4. Longrich, N.R., Martill, D.M., and Andres, B. (2018). Late Maastrichtian pterosaurs from North Africa and mass extinction of Pterosauria at the Cretaceous-Paleogene boundary. PLOS Biol. *16*, e2001663.
5. Venditti, C., Baker, J., Benton, M.J., Meade, A., and Humphries, S. (2020). 150 million years of sustained increase in pterosaur flight efficiency. Nature *587*, 83–86.
6. Butler, R.J., Benson, R.B.J., and Barrett, P.M. (2013). Pterosaur diversity: untangling the influence of sampling biases, Lagerstätten, and genuine biodiversity signals. Palaeogeogr. Palaeoclimatol. Palaeoecol. *372*, 78–87.
7. Butler, R.J., Brusatte, S.L., Andres, B., and Benson, R.B. (2012). How do geological sampling biases affect studies of morphological evolution in deep time? A case study of pterosaur (Reptilia: Archosauria) disparity. Evolution *66*, 147–162.
8. Prentice, K.C., Ruta, M., and Benton, M.J. (2011). Evolution of morphological disparity in pterosaurs. J. Syst. Palaeontol. *9*, 337–353.
9. Dyke, G.J., Mcgowan, A.J., Nudds, R.L., and Smith, D. (2009). The shape of pterosaur evolution: evidence from the fossil record. J. Evol. Biol. *22*, 890–898.
10. Foth, C., Brusatte, S.L., and Butler, R.J. (2012). Do different disparity proxies converge on a common signal? Insights from the cranial morphometrics and evolutionary history of Pterosauria (Diapsida: Archosauria). J. Evol. Biol. *25*, 904–915.
11. Benson, R.B., Frigot, R.A., Goswami, A., Andres, B., and Butler, R.J. (2014). Competition and constraint drove Cope's rule in the evolution of giant flying reptiles. Nat. Commun. *5*, 3567.
12. Butler, R.J., Barrett, P.M., Nowbath, S., and Upchurch, P. (2009). Estimating the effects of sampling biases on pterosaur diversity patterns: implications for hypotheses of bird/pterosaur competitive replacement. Paleobiology *35*, 432–446.
13. Sakamoto, M., Benton, M.J., and Venditti, C. (2016). Dinosaurs in decline tens of millions of years before their final extinction. Proc. Natl. Acad. Sci. USA *113*, 5036–5040.
14. Herrera-Flores, J.A., Elsler, A., Stubbs, T.L., and Benton, M.J. (2022). Slow and fast evolutionary rates in the history of lepidosaurs. Palaeontology *65*, e12579.
15. Witton, M.P. (2013). Pterosaurs: Natural History, Evolution, Anatomy (Princeton University Press).
16. Foth, C., Sookias, R.B., and Ezcurra, M.D. (2021). Rapid initial morphospace expansion and delayed morphological disparity peak in the first 100 million years of the archosauromorph evolutionary radiation. Front. Earth Sci. *9*, 723973.
17. Upham, N.S., Esselstyn, J.A., and Jetz, W. (2019). Inferring the mammal tree: species-level sets of phylogenies for questions in ecology, evolution, and conservation. PLoS Biol. *17*, e3000494.
18. Pyron, R.A., Burbrink, F.T., and Wiens, J.J. (2013). A phylogeny and revised classification of Squamata, including 4161 species of lizards and snakes. BMC Evol. Biol. *13*, 93.
19. Wiens, J.J. (2017). What explains patterns of biodiversity across the Tree of Life? BioEssays *39*, 1600128.
20. Britt, B.B., Dalla Vecchia, F.M., Chure, D.J., Engelmann, G.F., Whiting, M.F., and Scheetz, R.D. (2018). Caelestiventus hanseni gen. et sp. nov. extends the desert-dwelling pterosaur record back 65 million years. Nat. Ecol. Evol. *2*, 1386–1392.
21. Martínez, R.N., Andres, B., Apaldetti, C., and Cerda, I.A. (2022). The dawn of the flying reptiles: first Triassic record in the southern hemisphere. Pap. Palaeontol. *8*, e1424.
22. Labandeira, C.C., Sepkoski, J.J., and John, J. (1993). Insect diversity in the fossil record. Science *261*, 310–315.
23. Bestwick, J., Unwin, D.M., Butler, R.J., and Purnell, M.A. (2020). Dietary diversity and evolution of the earliest flying vertebrates revealed by dental microwear texture analysis. Nat. Commun. *11*, 5293.
24. Zhou, X., Pêgas, R.V., Ma, W., Han, G., Jin, X., Leal, M.E.C., Bonde, N., Kobayashi, Y., Lautenschlager, S., Wei, X., et al. (2021). A new darwinopteran pterosaur reveals arborealism and an opposed thumb. Curr. Biol. *31*, 2429–2436.e7.
25. Unwin, D.M. (2006). The Pterosaurs: From Deep Time (Pi Press).
26. Andres, B., Clark, J., and Xu, X. (2014). The earliest pterodactyloid and the origin of the group. Curr. Biol. *24*, 1011–1016.
27. Navarro, C.A., Martin-Silverstone, E., and Stubbs, T.L. (2018). Morphometric assessment of pterosaur jaw disparity. R. Soc. Open Sci. *5*, 172130.
28. Cincotta, A., Nicolaï, M., Campos, H.B.N., McNamara, M., D'Alba, L., Shawkey, M.D., Kischlat, E.E., Yans, J., Carleer, R., Escuillié, F., and Godefroit, P. (2022). Pterosaur melanosomes support signalling functions for early feathers. Nature *604*, 684–688.
29. Lü, J., Unwin, D.M., Deeming, D.C., Jin, X., Liu, Y., and Ji, Q. (2011). An egg-adult association, gender, and reproduction in pterosaurs. Science *331*, 321–324.
30. Knell, R.J., Naish, D., Tomkins, J.L., and Hone, D.W.E. (2013). Sexual selection in prehistoric animals: detection and implications. Trends Ecol. Evol. *28*, 38–47.
31. Bestwick, J., Unwin, D.M., Butler, R.J., Henderson, D.M., and Purnell, M.A. (2018). Pterosaur dietary hypotheses: a review of ideas and approaches. Biol. Rev. Camb. Philos. Soc. *93*, 2021–2048.
32. Witton, M.P. (2008). A new approach to determining pterosaur body mass and its implications for pterosaur flight. Zitteliana *28*, 143–158.
33. Witton, M.P., Habib, M.B., and Laudet, V. (2010). On the size and flight diversity of giant pterosaurs, the use of birds as pterosaur analogues and comments on pterosaur flightlessness. PLoS One *5*, e13982.
34. Naish, D. (2014). The fossil record of bird behaviour. J. Zool. *292*, 268–280.
35. Voeten, D.F.A.E., Cubo, J., de Margerie, E., Röper, M., Beyrand, V., Bureš, S., Tafforeau, P., and Sanchez, S. (2018). Wing bone geometry reveals active flight in Archaeopteryx. Nat. Commun. *9*, 923.

36. Yu, Y., Zhang, C., and Xu, X. (2021). Deep time diversity and the early radiations of birds. Proc. Natl. Acad. Sci. USA *118*. e2019865118.
37. Benson, R.B.J., and Choiniere, J.N. (2013). Rates of dinosaur limb evolution provide evidence for exceptional radiation in Mesozoic birds. Proc. R. Soc. B. *280*, 20131780.
38. Wang, M., Lloyd, G.T., Zhang, C., and Zhou, Z. (2021). The patterns and modes of the evolution of disparity in Mesozoic birds. Proc. Biol. Sci. *288*, 20203105.
39. Jagielska, N., O'Sullivan, M., Funston, G.F., Butler, I.B., Challands, T.J., Clark, N.D.L., Fraser, N.C., Penny, A., Ross, D.A., Wilkinson, M., and Brusatte, S.L. (2022). A skeleton from the Middle Jurassic of Scotland illuminates an earlier origin of large pterosaurs. Curr. Biol. *32*, 1446–1453.e4.
40. Tennant, J.P., Mannion, P.D., Upchurch, P., Sutton, M.D., and Price, G.D. (2017). Biotic and environmental dynamics through the Late Jurassic-Early Cretaceous transition: evidence for protracted faunal and ecological turnover. Biol. Rev. Camb. Philos. Soc. *92*, 776–814.
41. Martin-Silverstone, E., Witton, M.P., Arbour, V.M., and Currie, P.J. (2016). A small azhdarchoid pterosaur from the latest Cretaceous, the age of flying giants. R. Soc. Open Sci. *3*, 160333.
42. Berv, J.S., and Field, D.J. (2018). Genomic signature of an avian lilliput effect across the K-Pg extinction. Syst. Biol. *67*, 1–13.
43. Raup, D.M., and Sepkoski, J.J. (1984). Periodicity of extinctions in the geologic past. Proc. Natl. Acad. Sci. USA *81*, 801–805.
44. Benton, M.J. (2015). Exploring macroevolution using modern and fossil data. Proc. R. Soc. B. *282*, 20150569.
45. Foote, M. (1997). The Evolution of Morphological Diversity. Annu. Rev. Ecol. Syst. *28*, 129–152.
46. Jernvall, J., Hunter, J.P., and Fortelius, M. (1996). Molar tooth diversity, disparity, and ecology in Cenozoic ungulate radiations. Science *274*, 1489–1492.
47. Brocklehurst, N., and Benson, R.J. (2021). Multiple paths to morphological diversification during the origin of amniotes. Nat. Ecol. Evol. *5*, 1243–1249.
48. Simões, T.R., Vernygora, O., Caldwell, M.W., and Pierce, S.E. (2020). Megaevolutionary dynamics and the timing of evolutionary innovation in reptiles. Nat. Commun. *11*, 3322.
49. Close, R.A., Friedman, M., Lloyd, G.T., and Benson, R.B. (2015). Evidence for a mid-Jurassic adaptive radiation in mammals. Curr. Biol. *25*, 2137–2142.
50. Rabosky, D.L., Santini, F., Eastman, J., Smith, S.A., Sidlauskas, B., Chang, J., and Alfaro, M.E. (2013). Rates of speciation and morphological evolution are correlated across the largest vertebrate radiation. Nat. Commun. *4*, 1958.
51. Ruta, M., Angielczyk, K.D., Fröbisch, J., and Benton, M.J. (2013). Decoupling of morphological disparity and taxic diversity during the adaptive radiation of anomodont therapsids. Proc. R. Soc. Lond. B *280*, 20132414.
52. Stubbs, T.L., Pierce, S.E., Elsler, A., Anderson, P.S.L., Rayfield, E.,J., and Benton, M.J. (2021). Ecological opportunity and the rise and fall of crocodylomorph evolutionary innovation. Proc. R. Soc. Lond. B *288*, 20210069.
53. Wesley-Hunt, G.D. (2005). The morphological diversification of carnivores in North America. Paleobiology *31*, 35–55.
54. Condamine, F.L., Guinot, G., Benton, M.J., and Currie, P.J. (2021). Dinosaur biodiversity declined well before the asteroid impact, influenced by ecological and environmental pressures. Nat. Commun. *12*, 3833.
55. Sakamoto, M., Benton, M.J., Venditti, C., et al. (2021). Strong support for a heterogeneous speciation decline model in Dinosauria: a response to claims made by Bonsor. R. Soc. Open Sci. *8*, 202143. 2020.
56. Bonsor, J.A., Barrett, P.M., Raven, T.J., and Cooper, N. (2020). Dinosaur diversification rates were not in decline prior to the K-Pg boundary. R. Soc. Open Sci. *7*, 201195.
57. Tennant, J.P., Mannion, P.D., and Upchurch, P. (2016). Sea level regulated tetrapod diversity dynamics through the Jurassic/Cretaceous interval. Nat. Commun. *7*, 12737.
58. Tennant, J.P., Mannion, P.D., and Upchurch, P. (2016). Environmental drivers of crocodyliform extinction across the Jurassic/Cretaceous transition. Proc. Biol. Sci. *283*, 20152840.
59. de Celis, A., Narváez, I., Arcucci, A., and Ortega, F. (2021). Lagerstätte effect drives notosuchian palaeodiversity (Crocodyliformes, Notosuchia). Hist. Biol. *33*, 3031–3040.
60. Mannion, P.D., Chiarenza, A.A., Godoy, P.L., and Cheah, Y.N. (2019). Spatiotemporal sampling patterns in the 230 million year fossil record of terrestrial crocodylomorphs and their impact on diversity. Palaeontology *62*, 615–637.
61. Close, R.A., Benson, R.B.J., Alroy, J., Behrensmeyer, A.K., Benito, J., Carrano, M.T., Cleary, T.J., Dunne, E.M., Mannion, P.D., Uhen, M.D., and Butler, R.J. (2019). Diversity dynamics of Phanerozoic terrestrial tetrapods at the local-community scale. Nat. Ecol. Evol. *3*, 590–597.
62. Benton, M.J. (2010). The origins of modern biodiversity on land. Philos. Trans. R. Soc. Lond. B Biol. Sci. *365*, 3667–3679.
63. Lloyd, G.T., Davis, K.E., Pisani, D., Tarver, J.E., Ruta, M., Sakamoto, M., Hone, D.W.E., Jennings, R., and Benton, M.J. (2008). Dinosaurs and the Cretaceous terrestrial revolution. Proc. Biol. Sci. *275*, 2483–2490.
64. Benton, M.J., Wilf, P., and Sauquet, H. (2022). The Angiosperm Terrestrial Revolution and the origins of modern biodiversity. New Phytol. *233*, 2017–2035.
65. Scotese, C.R. (2021). An atlas of Phanerozoic paleogeographic maps: the seas come in and the seas go out. Annu. Rev. Earth Planet. Sci. *49*, 679–728.
66. Matsumoto, H., Coccioni, R., Frontalini, F., Shirai, K., Jovane, L., Trindade, R., Savian, J.F., and Kuroda, J. (2022). Mid-Cretaceous marine Os isotope evidence for heterogeneous cause of oceanic anoxic events. Nat. Commun. *13*, 239.
67. Larson, R.L. (1991). Latest pulse of Earth: evidence for a mid-Cretaceous superplume. Geology *19*, 547–550.
68. Van Valkenburgh, B.V., Wang, X., and Damuth, J. (2004). Cope's rule, hypercarnivory, and extinction in North American canids. Science *306*, 101–104.
69. Longrich, N.R., Bhullar, B.S., and Gauthier, J.A. (2012). Mass extinction of lizards and snakes at the Cretaceous-Paleogene boundary. Proc. Natl. Acad. Sci. USA *109*, 21396–21401.
70. Brown, J.H. (1995). Macroecology (University of Chicago Press).
71. Cardillo, M., Mace, G.M., Jones, K.E., Bielby, J., Bininda-Emonds, O.R., Sechrest, W., Orme, C.D., and Purvis, A. (2005). Multiple causes of high extinction risk in large mammal species. Science *309*, 1239–1241.
72. Mannion, P.D., Benson, R.B.J., Carrano, M.T., Tennant, J.P., Judd, J., and Butler, R.J. (2015). Climate constrains the evolutionary history and biodiversity of crocodylians. Nat. Commun. *6*, 8438.
73. Chiarenza, A.A., Mannion, P.D., Lunt, D.J., Farnsworth, A., Jones, L.A., Kelland, S.J., and Allison, P.A. (2019). Ecological niche modelling does not support climatically-driven dinosaur diversity decline before the Cretaceous/Paleogene mass extinction. Nat. Commun. *10*, 1091.
74. Wu, W.H., Zhou, C.F., Brian, A., and Matt, F. (2017). The toothless pterosaur Jidapterus edentus (Pterodactyloidea: Azhdarchoidea) from the Early Cretaceous Jehol Biota and its paleoecological implications. PLoS One *12*, e0185486.
75. Bouckaert, R., Vaughan, T.G., Barido-Sottani, J., Duchêne, S., Fourment, M., Gavryushkina, A., Heled, J., Jones, G., Kühnert, D., and Maio, N.D. (2019). BEAST 2.5: an advanced software platform for Bayesian evolutionary analysis. PLoS Comput. Biol. *15*, e1006650.
76. Thiele, K. (1993). The holy grail of the perfect character: the cladistic treatment of morphometric data. Cladistics *9*, 275–304.
77. Wei, X., Pêgas, R.V., Shen, C., Guo, Y., Ma, W., Sun, D., and Zhou, X. (2021). Sinomacrops Bondei, a new anurognathid pterosaur from the Jurassic of China and comments on the group. PeerJ *9*, e11161.

78. Zhang, C., Stadler, T., Klopfstein, S., Heath, T.A., and Ronquist, F. (2016). Total-evidence dating under the fossilized birth-death process. Syst. Biol. *65*, 228–249.
79. King, B., Qiao, T., Lee, M.S.Y., Zhu, M., and Long, J.A. (2017). Bayesian morphological clock methods resurrect placoderm monophyly and reveal rapid early evolution in jawed vertebrates. Syst. Biol. *66*, 499–516.
80. Lee, M.S.Y., Cau, A., Naish, D., and Dyke, G.J. (2014). Dinosaur evolution. Sustained miniaturization and anatomical innovation in the dinosaurian ancestors of birds. Science *345*, 562–566.
81. Brusatte, S.L., Lloyd, G.T., Wang, S.C., and Norell, M.A. (2014). Gradual assembly of avian body plan culminated in rapid rates of evolution across the dinosaur-bird transition. Curr. Biol. *24*, 2386–2392.
82. Zhang, C., and Wang, M. (2019). Bayesian tip dating reveals heterogeneous morphological clocks in Mesozoic birds. R. Soc. Open Sci. *6*, 182062.
83. Moon, B.C., and Stubbs, T.L. (2020). Early high rates and disparity in the evolution of ichthyosaurs. Commun. Biol. *3*, 68.
84. Fischer, V., Bardet, N., Benson, R.B.J., Arkhangelsky, M.S., and Friedman, M. (2016). Extinction of fish-shaped marine reptiles associated with reduced evolutionary rates and global environmental volatility. Nat. Commun. *7*, 1–11.
85. Simões, T.R., and Pierce, S.E. (2021). Sustained high rates of morphological evolution during the rise of tetrapods. Nat. Ecol. Evol. *5*, 1403–1414.
86. Ezcurra, M.D., Nesbitt, S.J., Bronzati, M., Dalla Vecchia, F.M., Agnolin, F.L., Benson, R.B.J., Brissón Egli, F., Cabreira, S.F., Evers, S.W., Gentil, A.R., et al. (2020). Enigmatic dinosaur precursors bridge the gap to the origin of Pterosauria. Nature *588*, 445–449.
87. Fischer, V., Benson, R.B.J., Zverkov, N.G., Soul, L.C., Arkhangelsky, M.S., Lambert, O., Stenshin, I.M., Uspensky, G.N., and Druckenmiller, P.S. (2017). Plasticity and convergence in the evolution of short-necked plesiosaurs. Curr. Biol. *27*, 1667–1676.e3.
88. Mao, F., Zhang, C., Liu, C., and Meng, J. (2021). Fossoriality and evolutionary development in two Cretaceous mammaliamorphs. Nature *592*, 577–582.
89. Zhou, C.F., Bhullar, B.-A.S., Neander, A.I., Martin, T., and Luo, Z.X. (2019). New Jurassic mammaliaform sheds light on early evolution of mammal-like hyoid bones. Science *365*, 276–279.
90. Cooney, C.R., Bright, J.A., Capp, E.J.R., Chira, A.M., Hughes, E.C., Moody, C.J.A., Nouri, L.O., Varley, Z.K., and Thomas, G.H. (2017). Mega-evolutionary dynamics of the adaptive radiation of birds. Nature *542*, 344–347.
91. Felice, R.N., and Goswami, A. (2018). Developmental origins of mosaic evolution in the avian cranium. Proc. Natl. Acad. Sci. USA *115*, 555–560.
92. Venditti, C., Meade, A., and Pagel, M. (2011). Multiple routes to mammalian diversity. Nature *479*, 393–396.
93. Rabosky, D.L., Grundler, M., Anderson, C., Title, P., Shi, J.J., Brown, J.W., Huang, H., and Larson, J.G. (2014). BAMMtools: an R package for the analysis of evolutionary dynamics on phylogenetic trees. Methods Ecol. Evol. *5*, 701–707.
94. Cui, X., Friedman, M., Qiao, T., Yu, Y., and Zhu, M. (2022). The rapid evolution of lungfish durophagy. Nat. Commun. *13*, 2390.
95. Louca, S., and Pennell, M.W. (2020). Extant timetrees are consistent with a myriad of diversification histories. Nature *580*, 502–505.
96. Louca, S., McLaughlin, A., MacPherson, A., Joy, J.B., and Pennell, M.W. (2021). Fundamental identifiability limits in molecular epidemiology. Mol. Biol. Evol. *38*, 4010–4024.
97. Stadler, T., Kühnert, D., Bonhoeffer, S., and Drummond, A.J. (2013). Birth-death skyline plot reveals temporal changes of epidemic spread in HIV and hepatitis C virus (HCV). Proc. Natl. Acad. Sci. USA *110*, 228–233.
98. Morlon, H., Robin, S., and Hartig, F. (2022). Studying speciation and extinction dynamics from phylogenies: addressing identifiability issues. Trends Ecol. Evol. *37*, 497–506.
99. Silvestro, D., Tejedor, M.F., Serrano-Serrano, M.L., Loiseau, O., Rossier, V., Rolland, J., Zizka, A., Höhna, S., Antonelli, A., and Salamin, N. (2019). Early arrival and climatically-linked geographic expansion of new world monkeys from tiny African ancestors. Syst. Biol. *68*, 78–92.
100. May, M.R., Contreras, D.L., Sundue, M.A., Nagalingum, N.S., Looy, C.V., and Rothfels, C.J. (2021). Inferring the total-evidence timescale of marattialean fern evolution in the face of model sensitivity. Syst. Biol. *70*, 1232–1255.
101. Andréoletti, J., Zwaans, A., Warnock, R.C.M., Aguirre-Fernández, G., Barido-Sottani, J., Gupta, A., Stadler, T., and Manceau, M. (2022). The occurrence birth–death process for combined-evidence analysis in macroevolution and epidemiology. Syst. Biol. *71*, 1440–1452.
102. Warnock, R.C.M., Heath, T.A., and Stadler, T. (2020). Assessing the impact of incomplete species sampling on estimates of speciation and extinction rates. Paleobiology *46*, 137–157.
103. Luo, A., Duchêne, D.A., Zhang, C., Zhu, C.D., and Ho, S.Y.W. (2020). A simulation-based evaluation of tip-dating under the fossilized birth–death process. Syst. Biol. *69*, 325–344.
104. Lloyd, G.T. (2018). Journeys through discrete-character morphospace: synthesizing phylogeny, tempo, and disparity. Palaeontology *61*, 637–645.
105. Lloyd, G.T. (2016). Estimating morphological diversity and tempo with discrete character-taxon matrices: implementation, challenges, progress, and future directions. Biol. J. Linn. Soc. Lond *118*, 131–151.
106. Guillerme, T., Puttick, M.N., Marcy, A.E., and Weisbecker, V. (2020). Shifting spaces: which disparity or dissimilarity measurement best summarize occupancy in multidimensional spaces? Ecol. Evol. *10*, 7261–7275.
107. Guillerme, T., and Cooper, N. (2018). Time for a rethink: time sub-sampling methods indisparity-through-time analyses. Palaeontology *61*, 481–493.
108. Foth, C., Ascarrunz, E., and Joyce, W.G. (2017). Still slow, but even steadier: an update on the evolution of turtle cranial disparity interpolating shapes along branches. R. Soc. Open Sci. *4*, 170899.
109. Henderson, D.M. (2010). Pterosaur body mass estimates from three-dimensional mathematical slicing. J. Vertebr. Paleontol. *30*, 768–785.
110. Baker, J., Meade, A., Pagel, M., and Venditti, C. (2015). Positive phenotypic selection inferred from phylogenies. Biol. J. Linn. Soc. Lond *118*, 95–115.
111. Naish, D., Witton, M.P., and Martin-Silverstone, E. (2021). Powered flight in hatchling pterosaurs: evidence from wing form and bone strength. Sci. Rep. *11*, 13130.

Please cite this article in press as: Yu et al., Complex macroevolution of pterosaurs, Current Biology (2023), https://doi.org/10.1016/j.cub.2023.01.007

STAR★METHODS

KEY RESOURCES TABLE

REAGENT or RESOURCE	SOURCE	IDENTIFIER
Deposited data		
Complete informal supertree (CIS)	This study	Online Data S1
parsimony strict consensus tree (PSC)	This study	Online Data S2
pruned informal supertree (PIS)	This study	Online Data S3
Expanded character matrix	This study	Online Data S4
Limb bone measurement dataset	This study	Online Data S5
Estimated log_{10} body mass	This study	Table S4
Figures and results for other sensitive analyses and statistical comparisons	This study	Online supplementary figures and results
Software and algorithms		
Beast2.6	https://www.beast2.org/	N/A
R.4.1.0	https://cran.r-project.org/	N/A
BayesTraitV3	http://www.evolution.reading.ac.uk/index.html	N/A
Mesquite 3.6	http://www.mesquiteproject.org/	N/A
Tracer	https://beast.community/tracer.html	N/A
TNT 1.5	www.lillo.org.ar/phylogeny/tnt/	N/A

RESOURCE AVAILABILITY

Lead contact

Further information and requests for resources should be directed to and will be fulfilled by the lead contact, Xing Xu (xu.xing@ivpp.ac.cn) or Chi Zhang (zhangchi@ivpp.ac.cn).

Materials availability

This study does not generate new fossil materials.

Data and code availability

Online Data S1–S5 are available at Figshare (https://figshare.com/s/78d52da7c58c396244f5). The non-phylogenetic regression and phylogenetic regression equation for log_{10} transformed body mass estimation and the estimated 120 log_{10} transformed body mass data are included as supplemental information with this article (Table S4). Figures and results for other sensitive analyses of diversification rates (Online Figures S3–S12), morphological rates (Online Figures S13–S20), morphological disparity (Online Figures S21–S25), body mass macroevolution (Online Figures S37–S43; Online Table S5), Correlation test with sampling proxies (Online Figures S26–S36), statistical comparison of the morphological (Online Tables S2–S4) and body mass disparities (Online Table S6), and a summary figure (Online Figure S44) are combined as a PDF file "online supplementary figures and results" (Online Tables S1–S6; Online Figures S1–S44), which is available on FigShare (at https://doi.org/10.6084/m9.figshare.19093877). The R code, Beast and BayesTrait scripts usedin this study are available on FigShare (at https://doi.org/10.6084/m9.figshare.19093877).

EXPERIMENTAL MODEL AND SUBJECT DETAILS

The character scoring information of the expanded character matrix was taken from references.[1,4,24,74] The limb bone measurements were taken from Benson et al.[11] and other published studies (see the citations in the legend of Figure S1). The informal supertrees were assembled according to published phylogenies (see the citations in the legend of Figure S1). The nexus files for the expanded character matrix and tree topologies are available as Online Data S1–S4, and limb bone measurements are available as Online Data S5 (deposit on Figshare https://doi.org/10.6084/m9.figshare.19093877).

METHOD DETAILS

Supertree assembly and data matrix construction

We first manually assembled a complete informal supertree (CIS) based on the phylogenetic framework in Longrich et al.[4] with additional 84 species added in (213 OTUs, including 212 pterosaurs and 1 outgroup species, covering nearly 87% of the known pterosaur species). 76 of the 84 OTUs were grafted onto the backbone tree based on published pterosaur phylogenies and 8 of the 84 OTUs, which have never been included in any numerical phylogenetic analysis, were grafted onto the backbone tree based on the phylogenetic positions of other species of the same genus that have been included in previous numerical phylogenetic analyses. Among the 84 species, 27 species were scored into the character matrix in Longrich et al.[4] with information from Zhou et al.[1,24] and Wu et al.,[74] and 57 species were coded as "?" for all characters. We then obtained a pruned informal supertree (PIS) tree from the CIS tree by deleting the 57 species with only "?" scorings (Online Figures S1 and S2). Finally, we obtained a parsimony strict consensus tree (PSC) by running a parsimony analysis on the character matrix containing only the species from PIS tree in TNT 1.5 with the same settings as in Longrich et al.[4] A simplified working flow is given in Figure S1 and all quantitative methods will be described specifically in "quantification and statistical analysis".

QUANTIFICATION AND STATISTICAL ANALYSIS

Morphological and diversification rate analyses

Inference of the morphological evolutionary rate and lineage diversification rate changing over time was performed in a coherent Bayesian tip dating framework using BEAST 2.6.0.[75] We performed the analyses on each of the three tree topologies based on both the unpartitioned and partitioned matrix (158 characters for CSR, 24 characters for ASR, 56 characters for PFR, and 32 characters for PHR). As continuous characters were not supported in BEAST 2, each of them was discretized into six states using the gap-weighting method.[7,76,77] This method also has been used for dealing with continuous characters in previous pterosaurs macroevolutionary analyses.[7,77] All 51 discretized continuous characters and 32 discrete characters were treated as ordered following Butler et al.,[7] Longrich et al.,[4] Thiele,[76] and Wei et al.,[77] and the rest of the discrete characters were unordered. The Markov k-states variable model (Mkv) with gamma-rate variation across all characters was used for the likelihood calculation. We used the skyline fossilized birth-death (SFBD) model[78] for the timetree. Each fossil age was assigned a uniform distribution with the data collected from the Paleobiology database (PBDB). The root age was assigned a uniform prior, *U* (238, 245), referring to the time range of the outgroup. Time was divided into 18 equal-duration intervals of 10 Myr each (with the first shift at 235 Ma and the last at 75 Ma; Figures 1, S2, and Online Figures S3–S7). The same diffuse exponential prior, Exp (20), was used for the speciation rate, extinction rate and fossilization rate in each time interval. We used the independent lognormal relaxed clock model for the evolutionary rates. The variance parameter of the clock was unlinked to allow evolutionary rate heterogeneity across different partitions. The mean (base) evolutionary rate was assigned a weakly informative lognormal(−4.5, 2.2) prior and each variance parameter was assigned a Gamma(0.5396, 0.3819) prior by default. To examine the robustness of the diversification dynamic pattern we observed in previous analyses, we repeated our analyses with the PSC topology using Exp (2) as the prior for the SFBD rate parameters. We also ran the diversification rate analyses using 5 Myr for each time bin to test robustness of the recovered diversification rate change pattern (Online Figures S8–S12). Time dependent morphological rate was summarized from tip dating results based on the PIS tree and the PSC tree.

The matrix we used in this study includes 60% missing data, which is a typical amount among the morphological matrices used in previous paleobiological macroevolutionary studies (e.g., 70% in a data matrix of early vertebrates[79]; 70% or 66% in Coelurosaurian theropods[80,81]; 50% in Mesozoic birds[82]; 52% or 45% in ichthyosaurs[83,84]; 59% in early amniotes[47]; 42% in early tetrapodomorphs[85]; 63% in early pterosaurs and lagerpetids[86]; 52% in Plesiosaurs[87]; 53% or 51% in mammals[88,89]). Following the strategy in previous studies,[17,18] we empirically test the correlation between the branch length/morphological rate (using $\mathrm{Log_e}$ transformed or non-transformed branch length and rate as dependent variable) for each terminal branch and the missing data proportion of each tip. The statistical tests of the slope of nearly all phylogenetic general least square regression (PGLS) models are non-significant. The R^2 and adjusted R^2 of all models are close to zero, meaning that the variation of rate and branch length of terminal branches are barely explained by the missing proportion, supporting that missing data do not consistently bias rate and branch length estimation (Table S1).

Following the method mostly used in previous studies,[90–94] the rate at each time point is summarized as the mean rate across all branches at that time point. We randomly sampled 1500 trees from the posterior tree sample, and for each tree, we calculated the mean rate across all branches at each time point of 1 Ma increment from 66 Ma to 245 Ma. Over the 1500 trees, we summarized the mean rates at each time point with median and upper (3/4) and lower (1/4) quartiles (Online Figures S13–S16 for morphological through time plot and Online Figures S17–S20 for morphological rate mapping on tree). PD curve was summarized with the tip-dated CIS tree. The median number of lineages and the upper and lower quartiles at each time points were summarized with the 1500 sampled posterior trees.

One major concern is unidentifiable issues in the birth-death models. However, we note that the recent mathematical results are for ultrametric trees (trees with only extant taxa).[95] For trees with serially sampled tips, the birth-death-sampling model widely used in epidemiology also has unidentifiable issues,[96,97] as the model assumes that upon sampling the lineage is dead, thus sampling and death has indistinguishable effects. For the SFBD model with fossil samples (each being either a tip or an ancestor), none

unidentifiable issue has been discovered or mathematically proved.[98] Even if unidentifiable issues exist, Bayesian analyses through the use of priors can greatly alleviate unidentifiability.[98] Several case studies have used the SFBD method variants to detect tempo and mode of diversification dynamics in deep time,[36,85,99–101] and there are studies (including simulation study) demonstrating that diversification rate estimates under the FBD model are robust despite fossil data are sparse.[78,100–103] In our analyses, we have included pterosaur species as many as possible and recovered similar patterns of speciation, extinction, and fossil-sampling rates changing through time under two different priors (exp(2) and exp(20)) and three different trees (CIS, PSC and PIS) with different number of taxon sampling, demonstrating the robustness of our results. These trees different in size to some extent also accounted for the potential impact of biased or limited fossil sampling. However, a thorough investigation of fossil sampling issues on birth-death rates requires further extensive computer simulations.

Morphological disparity analyses

We employed a phylomorphospace approach to include internal nodes into our morphological disparity analyses. Due to the similarity of the estimated node ages among different tip dating models, we only used the output Maximum clade credibility trees based on unpartitioned analyses with the PIS tree and the PSC tree. We estimated the ancestral character states for the internal nodes with a recently developed pre-OASE1 method, which can minimize the introduced phylogenetic signal and provide a better approximation to the true morphospace compared with other phylomorphospace approaches[104] (Table 1; Lloyd[104]). The maximum observable distance (MORD) matrix was used for disparity analyses. Comparing with general Euclidean distance (GED) used in previous pterosaur macroevolutionary analyses,[6–8] MORD provide higher fidelity under missing data.[105] The principal coordinate analyses (PcoA) were performed to ordinate all tips and internal nodes into a multivariate morphospace. The sum of variances (measuring the size of morphospace)[106] on all axes that together comprise 90% of total variance was used as the measure of morphological disparity. This disparity metric is relatively robust to sample size.[7,48]

We adopted three post-ordination approaches to summarize the time dependent disparity of the whole skeleton. We first used a time-bin method by subdivided time into 17 equal-duration intervals of 10 Myr each as in our tip dating analyses. The disparity metric in each time bin was calculated using coordinates of the tips and ancestral nodes within the corresponding bin. The distribution of the disparity metric in each time bin was simulated by 500 bootstraps. We also performed subsampled disparity curves using rarefication analyses with time-bin method. Disparity of each time-bin were subsampled at a sample size of 5^4. The sample size of the last time bin (the 75–66 bin) is smaller than 5, so the 85–75 and 75–66 bins were combined into a single bin with a sample size of ten (following the strategy used in Butler et al.[7]). These curves were given in Online Figure S23. Then we used two variants of the time-slicing method, that is, the equal split and gradual split models.[107] These time-slicing methods not only consider internal nodes and tips, but also branch length information, which can inflate the sample through time and avoid disparity gaps for those time periods with poor fossil records.[107,108] The time slices were taken as 16 equidistant time points of 10 Myr. The distribution of disparity metric at each time point was simulated with 100 bootstraps, with rarefaction limits the number of elements drawn from each bootstrap replication (Using the function ''boot.matrix'' in package ''dispRity'' with ''rarefaction'' setting to TRUE). We also used an alternative way to get the distribution of disparity metric, that is, we sampled 100 posterior trees, and for each tree, we summarized the median disparity metric at each time point for each rarefaction. Finally, we repeated our analyses with the weighted mean pairwise distance (WMPD)[49] (measuring the density of morphospace),[106] which is robust to sample size.[49] We performed Mann-Whitney-Wilcoxon tests and permutation tests for morphological disparity comparison over time.

We further summarized the disparity curve for each anatomical subregions (the same partition as in morphological evolutionary rate analyses). Due to the reduction of sample size for several subregions and time-bin method will generate disparity gap, we only used the two variants of the time-slice method to avoid disparity gaps in the curve. Then we performed correlation test (using Spearman's rank) between disparity curves of different anatomical subregions using the median value at each time point. The data were detrended with generalized differencing before analyses, which can remove trends and autocorrelation in time series data (Online Table S4; Online Figures S24 and S25).

Finally, we compared disparity among different Pterosauria groups. The tips and internal nodes were divided into 4 groups, that is, the non-Pterodactyloidea pterosaurs, Archaeopterodactyloidea, Pteranodontia and Azhdarchoidea.

Correlation test with sampling proxies

Previous studies have shown that pterosaur taxonomic diversity counts were biased by stratigraphic sampling proxies. We performed correlation tests between diversification dynamic parameters (using speciation, extinction and net lineage diversification rates from the posterior distributions) and stratigraphic sampling proxies (pterosaur-bearing formations and pterosaur-bearing collections), between median morphological disparity (the median disparity metric from the distribution simulated by bootstraps) and stratigraphic sampling proxies using Pearson's product-moment, Spearman's rank, and Kendall's tau. Analyses were performed in R 4.1.0. Data of pterosaur-bearing formations and pterosaur-bearing collections were downloaded from PBDB in July 2021. All time series data were detrended using generalized differencing method before the correlation tests. This is because time series data often have overall trend and thus easily induce positive or negative correlation. Results of correlation tests between morphological disparity and sampling proxies are given in Table S2, and others are given in Figures S3 and Online Figures S26–S36.

Body mass estimation

There are some published pterosaur body mass data,[32,109] but they are either limited in taxonomical sampling or criticized as inaccurate.[33] The largest published dataset of pterosaur body mass, which contains 75 species, is based on wingspan data, considered as a good predictor for pterosaur body mass.[5] However, the reconstruction of wing configurations is often subjective, and only a small number of pterosaur specimens preserve complete wing. For instance, the wingspan data used in Venditti et al.[5] are derived from Benson et al.,[11] in which only 34 taxa are represented by complete forelimb elements, and other wingspan data in this dataset were estimated using regression model or non-statistical method, and furthermore, some models' R^2 are relatively low.[11]

In order to obtain reliable body mass data, we developed a new method. More specifically, we performed preliminary ordinary least squares (OLS) regression between different limb bone measurements (Length measurements of selected limb bones, including humerus, ulna, wing metacarpal, femur, and tibia) and reliable body mass data of 19 pterosaurs that are estimated based on the relationship between dry skeletal mass and body mass[32] (Body mass data of this study have been widely accepted and cited), which indicates strong correlations between the measurements and body mass (Table S3).

We then performed Bayesian phylogenetic generalized least square (PGLS) regression to select the best-fitting model among five models, including Brownian Motion (BM), lambda, kappa, delta, and Ornstein–Uhlenbeck (OU), for each predictive variable, using BayesTraitsV3 with default priors. The maximum clade credibility (MCC) trees with the 19 species were used to consider phylogenetic signal (CIS tree under 18 time-binned SFBD model with partitioned morphological rate analyses). Each analysis was run 5 million iterations and sampled every 5000 iterations. The first 25% samples were discarded as burn-in. Convergence of parameters was identified using Tracer as ESS > 100. Marginal likelihood (log base 10) of each model was calculated using stepping-stone algorithm with 150 stones and 10000 iterations of each, and model selection was determined by logarithmic Bayes factor (difference of $\log_{10}$ marginal likelihoods). Our model test showed that using tree transformations would not increasing model fit significantly (log Bayes factor < 2). The best predictor for body mass is the combined lengths of humerus and ulna. Ulna length is also strongly correlated with body mass. Wing metacarpal has the weakest prediction compared with the other predictive variables, but also has a 0.88 median coefficient of determination.

We then collected limb bone measurements data from the published literatures (468 specimens were checked); We estimated the body mass of the 120 pterosaur species (covering about 49% of the known pterosaur species) using the Bayesian PGLS under the BM model (pre-selected according to Bayes factor) with default priors and the trees used for model fitting. Traditionally phylogenetic comparative method uses a single trait value for each species. In our dataset, most species are represented by a single specimen, but 28 pterosaur species have multiple specimens after removing juvenile individuals. For these species, the values of multiple specimens for the predictive variable were input into BayesTraitsV3, and they were integrated over in the inference. According to previous model selection results, we preferred estimating body mass with the following predictors: combined lengths of humerus and ulna (80 taxa), ulna length (9 taxa), humeral length (20 taxa), femoral length (1 taxa), tibial length (1 taxa), and wing metacarpal length (1 taxon), with the exception of *Caiuajara dobruskii*, *Ctenochasma elegans*, *Eudimorphodon ranzii* and *Nyctosaurus gracilis* in which using humerus length as a predictive variable can include much larger specimens. For the taxa used for model fitting with multiple specimens (11 taxa), we re-estimated their body mass with the Bayesian PGLS model. The estimated median body masses from convergent posterior distributions were taken as input in subsequent analyses.

Body mass macroevolutionary analyses

We use the $\log_{10}$ transformed body mass data as input for the following macroevolutionary analyses. Branch specific body mass evolutionary rates were estimated in BayesTraitV3 using default priors. The estimated median body mass for each pterosaur was taken as input. The variable rates model uses reversible jump Markov Chain Monte Carlo algorithm to detect regions of the tree (the same tree for PGLS model fit) that the evolutionary rate varies significantly.[92] We tested five models: single rate BM, variable rates BM, lambda, kappa and delta. We did not use the OU model because the variable rates+OU model is only available for ultrametric tree (See the manual of BayesTraitV3 page 48 and 60). Each analysis was run a billion iterations and sampled every 100000 iterations. The first 25% samples were discarded as burn-in. Convergence of parameters was identified using Tracer (ESS > 100). Marginal likelihood (log base 10) of each model was calculated using stepping-stone algorithm with 200 stones and 10000 iterations of each, and model selection was determined by logarithmic Bayes factor (difference of $\log_{10}$ marginal likelihoods). Results for model selection are given in Table S4. Most of the time, using kappa and lambda transformation leaded to a similar marginal likelihood. Branch specific mean rate scaler was summarized using The Variable Rates Post Processor.[110]

We then performed ancestral body mass reconstruction under BM model in BayesTraitV3 with the rescaled MCC trees in Output.trees file output from previous variable rate model analyses to account for the unequal rates of evolution across the tree and non-BM trait evolution.[90] Each analysis was run a 100 million iterations and sampled every 10000 iterations. The first 25% samples were discarded as burn-in. Convergence of parameters was identified using Tracer (ESS > 100). Variance was chosen as the disparity metric for body mass. Time dependent body mass disparity and mean body mass were summarized with both time-bin and time-slicing methods, as in the morphological disparity analyses (Figure 4). We used Mann-Whitney-Wilcoxon tests and permutation tests for statistical comparison of the body mass disparities between the two neighbored time bins/points.

We repeated the analyses described above with body mass data of the 19 pterosaurs for model fitting all taken from Witton.[32] A recently published study argued that *Nemicolopterus crypticus* is a hatchling,[111] which might bias our body mass macroevolutionary analyses, so we repeated all our analyses with this taxon deleted (Online Figures S37–S43).

Current Biology, Volume *33*

Supplemental Information

Complex macroevolution of pterosaurs

Yilun Yu, Chi Zhang, and Xing Xu

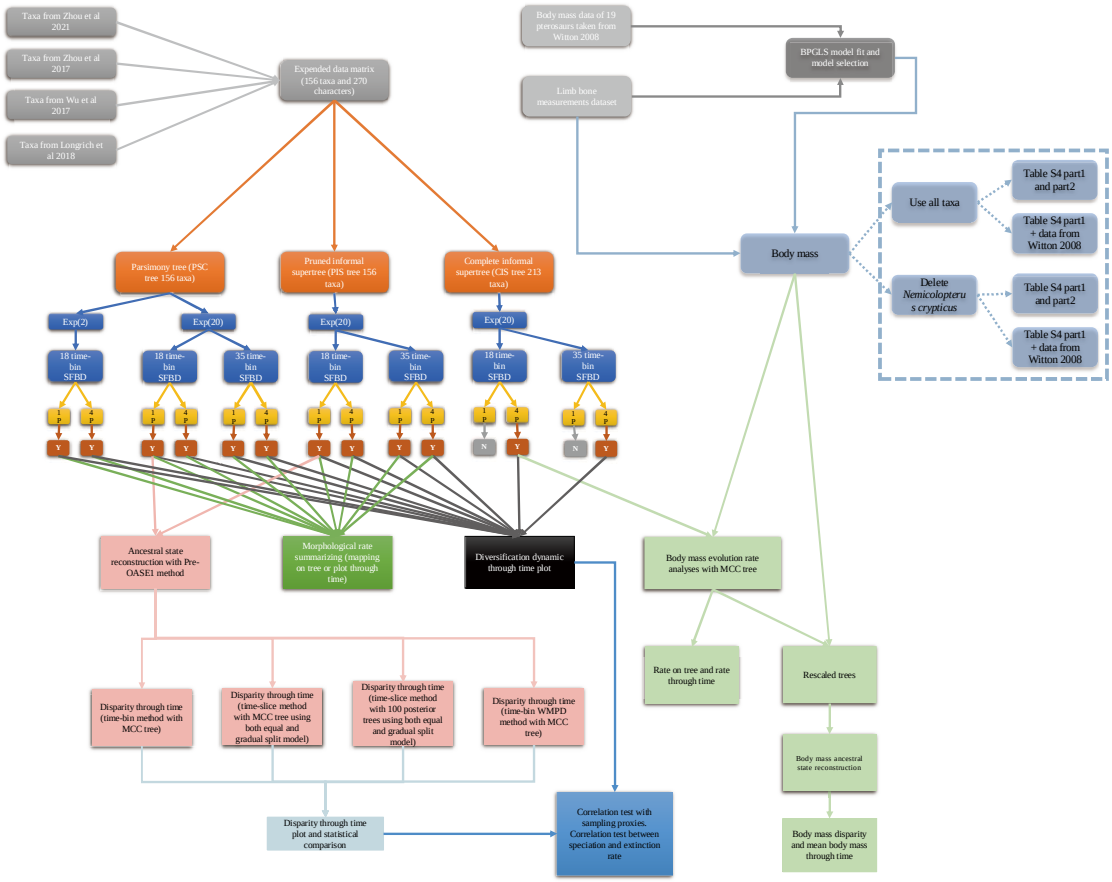

Figure. S1. Simplified experimental working flow. Relate to Figure 1.

Abbreviations: 1P, unpartitioned analysis; 4P, partitioned analysis; N, the MCMC was not converged; Y, the MCMC was converged. The Bayesian tip-dating analyses were performed on the three tree topologies and the expended data matrix, using different priors or SFBD model with different number of time intervals. For PSC and PIS tree, all models were converged, whereas, only the partitioned models were converged for the analyses based on CIS tree (assembled according to ref. [S1- S 23]). Then the diversification parameters were summarized with skyline plots for all converged models. Morphological rates were summarized only for the analyses based on PSC and PIS trees. Phylomorphospace for overall morphological disparity analyses were construct with the MCC trees output from unpartitioned analyses with PSC and PIS trees. Phylogenetic diversity curves were summarized from the posterior trees output from the converged model using CIS tree (not shown on the figure). The disparity metrics, diversification parameters and stratigraphic sampling proxies were detrended with generalized differencing and used as input for the correlation tests. The MCC tree output from partitioned data and SFBD model under the CIS tree (Partitioned+18 time-bin SFBD+CIS) was used for body mass macroevolutionary analyses. For body mass macroevolutionary analyses (Limb bone measurements were assembled according to ref. [S2, S4- S6, S10- S15, S17- S47]), we repeated all analyses under the conditions bounded by the dashed rectangle.

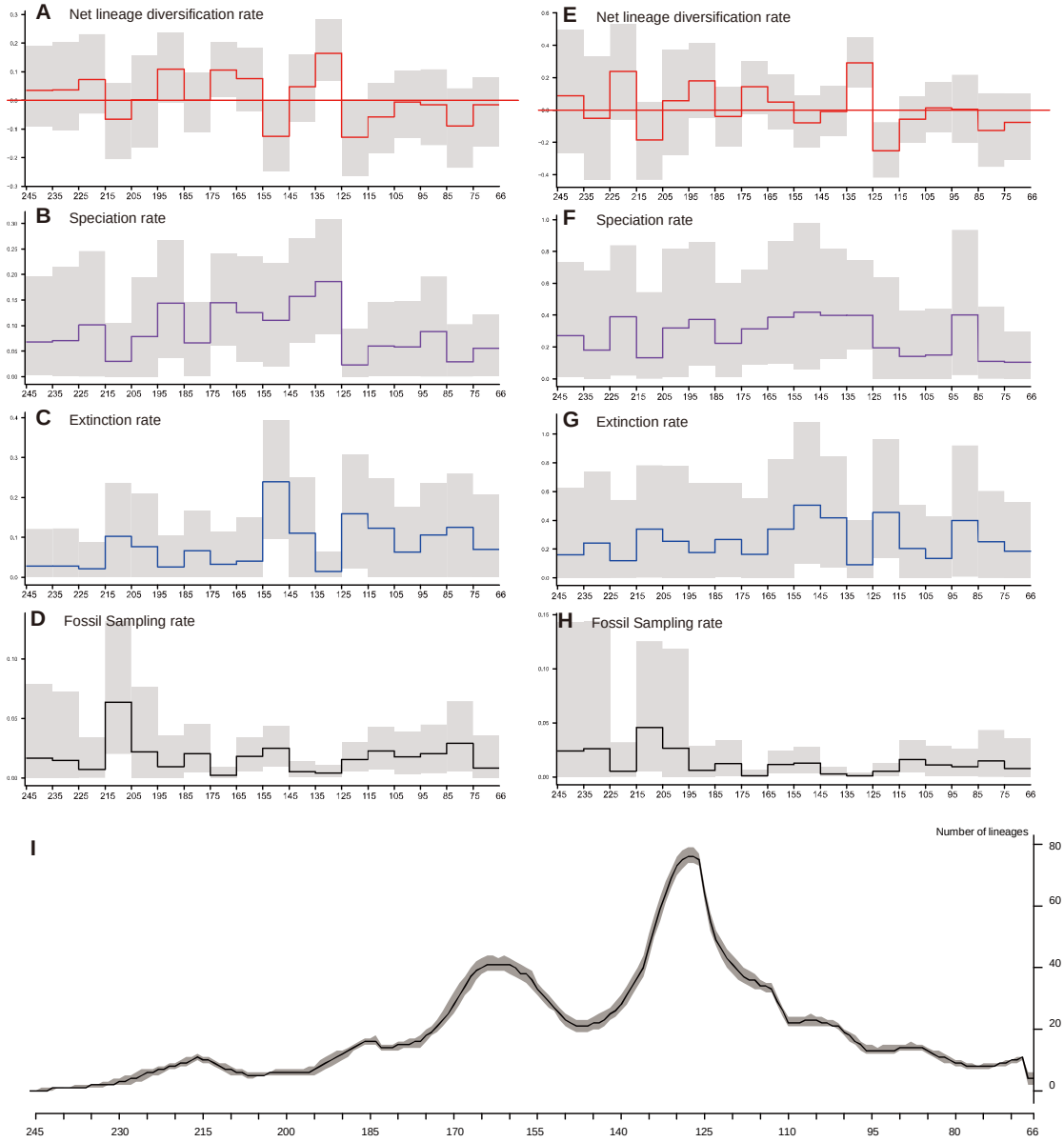

Figure. S2. Pterosaur diversity through time. Relate to Figure 1.

Diversification dynamic parameters estimated under the unpartitioned+SFBD+PSC model, the same Exp(20) prior was used for the speciation, extinction, and fossil-sampling rates (A-D). Sensitive analyses using Exp(2) as the prior for the speciation, extinction, and fossil-sampling rates (E-H). Net lineage diversification rate (A-E), speciation rate (B-F), extinction rate (C-G), and fossil-sampling rate (D-H). Phylogenetic diversity curve (I).

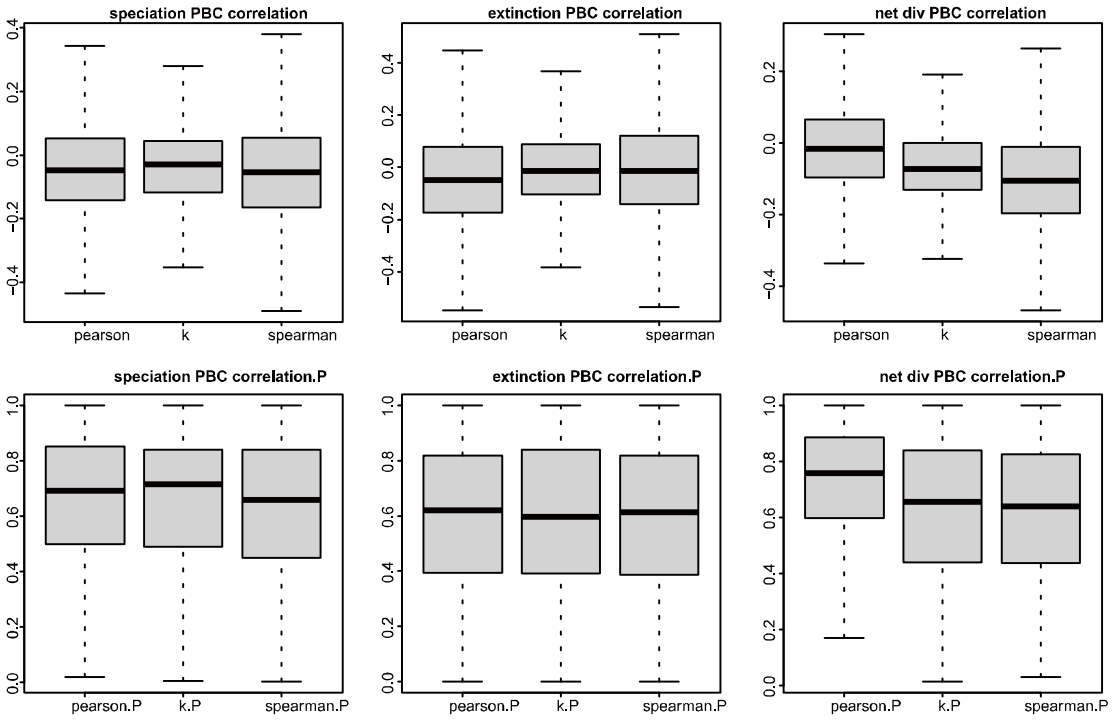

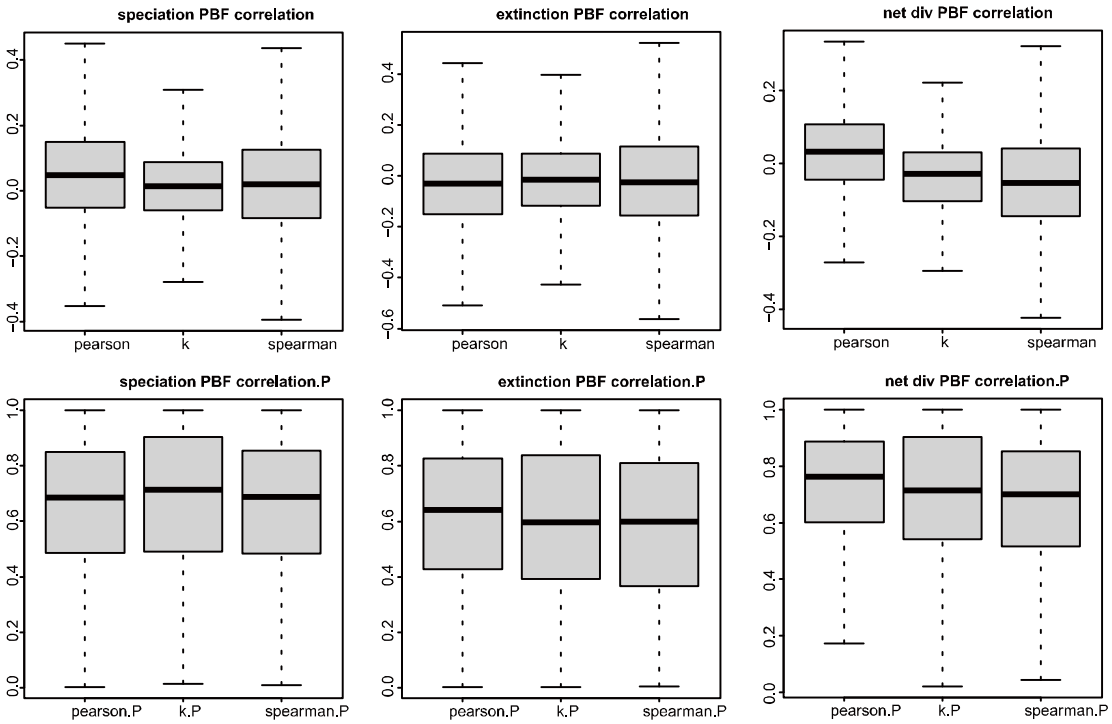

Figure. S3. P.values and correlation coefficients of correlation tests between diversification parameters and stratigraphic sampling proxies. Relate to Figure 1.

Diversification dynamic parameters were estimated under the partitioned+SFBD+CIS model. Test were performed on all samples from the converged posterior distribution.

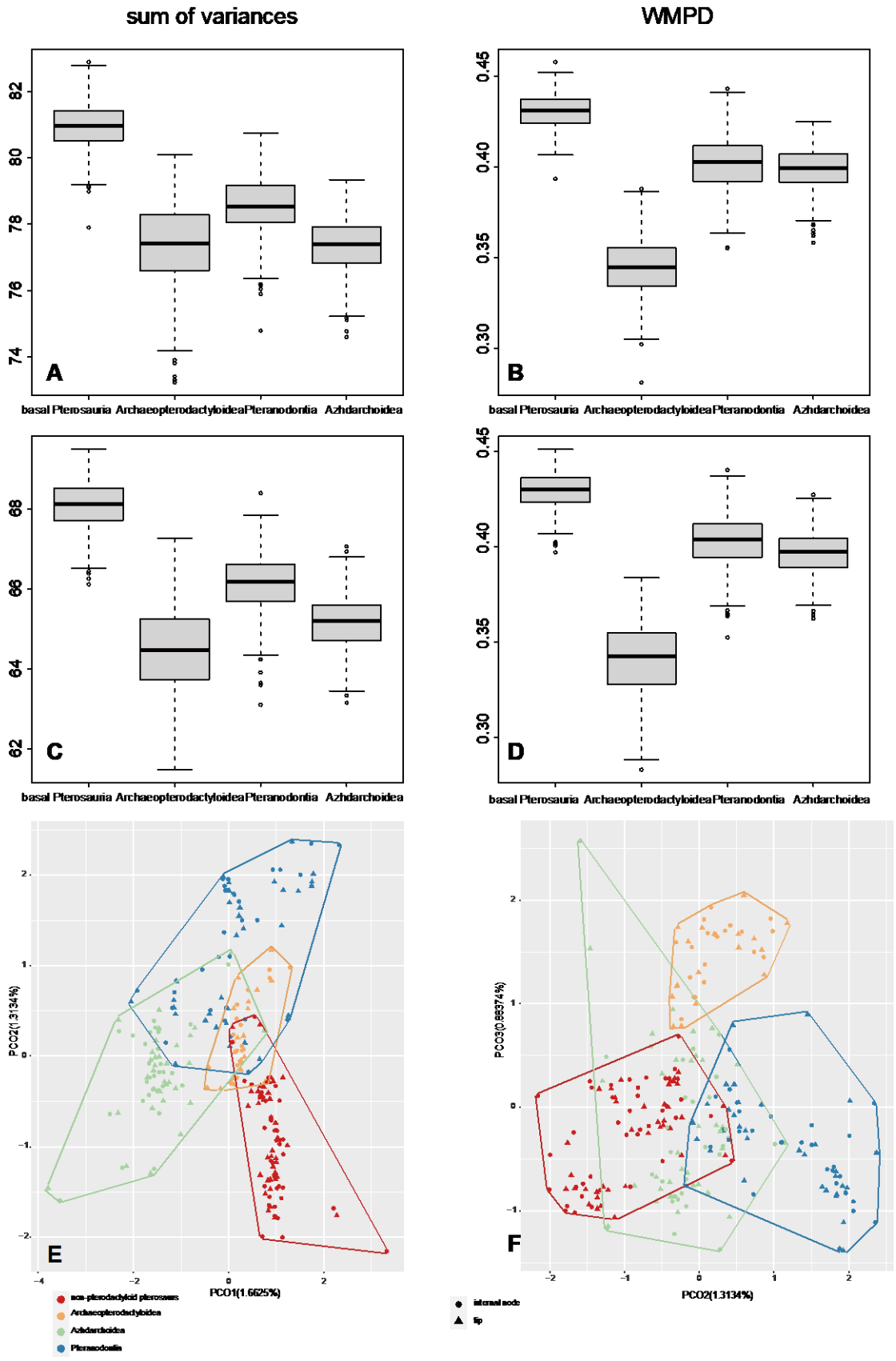

Figure S4. Pterosaur phylomorphospace and disparity comparison. Relate to Figure 3.

Comparison of morphological disparity between different groups. Unpartitioned+SFBD+PSC

model (A-B), unpartitioned+SFBD+PIS model (C-D). Phylomorphospace comparison of different group of pterosaurs shown by PCO1 and PCO2, and PCO2 and PCO3 (under unpartitioned+SFBD+PIS model) (E-F). We only show the first 3 PCO axes here, but the statistical analyses were performed on all axes that together comprise 90% of total variance.

Tree_model	Character partition	dependent variable	Slope	Slope P.value	R^2	Adjust R^2	Pagel's Lambda
PIS_unpartiton	unpartiton	Terminal branch length	-0.38331	0.86055	0.000201	-0.006291	1
		Terminal branch rate	0.0026150	0.4598	0.003553	-0.002917	0
		Log_e Terminal length	0.03265	0.9299	5.589e-05	-0.007138	0.712
		Log_e Terminal rate	0.29913	0.1851	0.01138	0.004956	0.087
PIS_partiton	skull	Terminal branch length	2.1416	0.30009	0.006971	0.0005228	1
		Terminal branch rate	-0.00076436	0.818	0.0003449	-0.006146	0
		Log_e Terminal length	0.45768	0.1716	0.01303	0.00613	0.788
		Log_e Terminal rate	0.076989	0.7012	0.0009586	-0.005529	0
	axial	Terminal branch length	-3.0735	0.09234	0.01829	0.01191	1
		Terminal branch rate	0.00028887	0.9009	0.0001011	-0.006392	0
		Log_e Terminal length	-0.40832	0.1208	0.01675	0.009876	0.8
		Log_e Terminal rate	0.184993	0.1495	0.01344	0.007035	0
	forelimb	Terminal branch length	-2.1504	0.25587	0.008375	0.001936	1
		Terminal branch rate	-0.0047588	0.1019	0.01728	0.01089	0.399
		Log_e Terminal length	-0.33284	0.2014	0.01139	0.004477	0.793
		Log_e Terminal rate	-0.15163	0.1434	0.01385	0.007451	1
	hindlimb	Terminal branch length	-1.8841	0.32535	0.006282	-0.000171	1
		Terminal branch rate	-0.0017363	0.4692	0.003408	-0.003064	0.159
		Log_e Terminal length	-0.40552	0.1165	0.01714	0.01027	0.796
		Log_e Terminal rate	0.07401	0.5273	0.0026	-0.003877	0.277
PSC_unpartiton	unpartiton	Terminal branch length	-0.65512	0.7780	0.0005179	-0.005972	1
		Terminal branch rate	0.00022314	0.9447	3.134e-05	-0.006462	0
		Log_e Terminal length	0.074232	0.8367	0.0003068	-0.006885	0.811
		Log_e Terminal rate	0.13562	0.5197	0.002696	-0.00378	0.112
PSC_partiton	skull	Terminal branch length	1.9373	0.31808	0.006473	2.129e-05	1
		Terminal branch rate	-0.0021357	0.4552	0.003626	-0.002844	0
		Log_e Terminal length	0.26004	0.4748	0.003577	-0.003391	0
		Log_e Terminal rate	-0.019155	0.9182	6.871e-05	-0.006424	0
	axial	Terminal branch length	-2.8666	0.12704	0.01505	0.008658	1
		Terminal branch rate	0.0002212	0.9287	5.21e-05	-0.006441	0
		Log_e Terminal length	-0.52457	0.082	0.021	0.01416	0
		Log_e Terminal rate	0.094270	0.4311	0.00403	-0.002437	0
	forelimb	Terminal branch length	-2.7661	0.12674	0.01508	0.008681	1
		Terminal branch rate	-0.0059461	0.03484	0.02859	0.02228	0
		Log_e Terminal length	-0.50983	0.0868	0.02037	0.01352	0
		Log_e Terminal rate	-0.099935	0.4091	0.00443	-0.002035	0
	hindlimb	Terminal branch length	-2.1455	0.23492	0.009149	0.002715	1
		Terminal branch rate	-0.0018755	0.394	0.004723	-0.00174	0.303
		Log_e Terminal length	-0.71939	0.009008	0.04674	0.04007	0
		Log_e Terminal rate	0.057289	0.615	0.001647	-0.004836	0.362
PSC_unpartiton	unpartiton	Terminal branch length	0.26901	0.9070	8.893e-05	-0.006404	1

exp2		Terminal branch rate	-8.4347e-05	0.9818	3.401e-06	-0.00649	0.085
		Log_e Terminal length	0.071918	0.8139	0.000368	-0.006252	0.927
		Log_e Terminal rate	0.066113	0.7638	0.0005879	-0.005902	0.205
PSC_partiton exp2	skull	Terminal branch length	3.5452	0.1043	0.01705	0.01066	1
		Terminal branch rate	-0.0025754	0.3948	0.004706	-0.001757	0
		Log_e Terminal length	0.60467	0.03771	0.02828	0.02185	0.828
		Log_e Terminal rate	-0.062233	0.7441	0.000694	-0.005795	0
	axial	Terminal branch length	-1.9087	0.29874	0.00701	0.000562	1
		Terminal branch rate	-0.00043572	0.8626	0.0001952	-0.006297	0
		Log_e Terminal length	-0.12707	0.5894	0.001934	-0.004676	0.813
		Log_e Terminal rate	0.099928	0.4296	0.004057	-0.00241	0.121
	forelimb	Terminal branch length	-1.5999	0.37302	0.005156	-0.001304	1
		Terminal branch rate	-0.0064027	0.03961	0.02721	0.02089	0.122
		Log_e Terminal length	-0.11720	0.612	0.001708	-0.004903	0.812
		Log_e Terminal rate	-0.075141	0.5658	0.002146	-0.004334	0.342
	hindlimb	Terminal branch length	-1.1380	0.51822	0.002716	-0.00376	1.000
		Terminal branch rate	-0.0022338	0.374	0.005136	-0.001324	0.198
		Log_e Terminal length	-0.14637	0.5145	0.00282	-0.003784	0.809
		Log_e Terminal rate	0.021507	0.856	0.0002144	-0.006278	0.324

Table S1. Empirical statistical test between terminal branch length/terminal branch rate and missing-data proportion of each tip. Relate to Figure 2.

Terminal branch rate or terminal branch length is dependent variable, and missing proportion is predictor variable.

Part1: correlation tests between median morphological disparity and sampling proxies				
Time-bin method				
time_bin	**SOV PSC**	**SOV PIS**	**WMPD PSC**	**WMPD PIS**
PBF Pearson	0.153	0.132	0.23	0.261
PBF Pearson P.value	0.587	0.64	0.392	0.329
PBF Kendall	0.0286	0.0476	0.183	0.2
PBF Kendall P.value	0.923	0.846	0.350	0.306
PBF Spearman	0.118	0.0464	0.282	0.294
PBF Spearman P.value	0.676	0.873	0.288	0.268
PBC Pearson	0.0382	0.012	0.154	0.207
PBC Pearson P.value	0.893	0.944	0.569	0.442
PBC Kendall	0.00952	0.0286	0.15	0.167
PBC Kendall P.value	1	0.923	0.450	0.398
PBC Spearman	0.0464	-0.0036	0.197	0.224
PBC Spearman P.value	0.873	0.995	0.463	0.404
Time-slice method with maximum clade credibility tree output from Bayesian tip-dating				
time_slice	**SOV Equal Split PSC**	**SOV Equal Split PIS**	**SOV Gradual Split PSC**	**SOV Gradual Split PIS**
PBF Pearson	0.288	0.162	0.322	0.188
PBF Pearson P.value	0.317	0.581	0.261	0.521
PBF Kendall	0.319	0.275	0.297	0.209
PBF Kendall P.value	0.127	0.193	0.157	0.331
PBF Spearman	0.481	0.380	0.446	0.244
PBF Spearman P.value	0.084	0.181	0.112	0.4
PBC Pearson	0.342	0.211	0.336	0.213
PBC Pearson P.value	0.232	0.4687	0.2395	0.4657
PBC Kendall	0.275	0.231	0.253	0.165
PBC Kendall P.value	0.193	0.279	0.233	0.451
PBC Spearman	0.429	0.319	0.354	0.213
PBC Spearman P.value	0.128	0.267	0.215	0.464
Time-slice method with 100 posterior trees output from Bayesian tip-dating				
time_slice	**SOV Equal Split PSC**	**SOV Equal Split PIS**	**SOV Gradual Split PSC**	**SOV Gradual Split PIS**
PBF Pearson	0.284	0.341	0.292	0.391
PBF Pearson P.value	0.326	0.233	0.31	0.167
PBF Kendall	0.187	0.363	0.253	0.407
PBF Kendall P.value	0.388	0.0795	0.233	0.0472
PBF Spearman	0.305	0.459	0.354	0.516
PBF Spearman P.value	0.288	0.101	0.215	0.0616
PBC Pearson	0.292	0.386	0.309	0.436
PBC Pearson P.value	0.310	0.173	0.282	0.119
PBC Kendall	0.143	0.319	0.209	0.363
PBC Kendall P.value	0.518	0.127	0.331	0.0795

PBC Spearman	0.191		0.415	0.275	0.464	
PBC Spearman P.value	0.512		0.141	0.341	0.0972	
Part2: P-values for statistical comparison of the disparities between different groups						
Mann-Whitney-Wilcoxon tests						
	basal: Archaeopterodactyloidea	**basal: Pteranodontia**	**basal: Azhdarchoidea**	**Archaeopterodactyloidea: Pteranodontia**	**Archaeopterodactyloidea: Azhdarchoidea**	**Pteranodontia: Azhdarchoidea**
SOV PSC	2.20E-16	2.20E-16	2.20E-16	2.20E-16	0.1471	2.20E-16
SOV PIS	2.20E-16	2.20E-16	2.20E-16	2.20E-16	2.20E-16	2.20E-16
WMPD PSC	2.20E-16	2.20E-16	2.20E-16	2.20E-16	2.20E-16	0.0001747
WMPD PIS	2.20E-16	2.20E-16	2.20E-16	2.20E-16	2.20E-16	1.96E-14
Permutation tests						
	basal: Archaeopterodactyloidea	**basal: Pteranodontia**	**basal: Azhdarchoidea**	**Archaeopterodactyloidea: Pteranodontia**	**Archaeopterodactyloidea: Azhdarchoidea**	**Pteranodontia: Azhdarchoidea**
SOV PSC	0.00E+00	0.00E+00	0.00E+00	0.00E+00	0.278	0.00E+00
SOV PIS	0.00E+00	0.00E+00	0.00E+00	0.00E+00	0.00E+00	0.00E+00
WMPD PSC	0.00E+00	0.00E+00	0.00E+00	0.00E+00	0.00E+00	5.00E-04
WMPD PIS	0.00E+00	0.00E+00	0.00E+00	0.00E+00	0.00E+00	0.00E+00

Table S2. P-values of correlation tests between median morphological disparity and sampling proxies, and disparity comparison among different groups. Relate to Figure 3.

Abbreviations: SOV, sum of variances; WMPD, weighted mean pair wise distance; PSC, parsimony strict consensus tree topology; PIS, pruned informal supertree.

Part1: Non-phylogenetic OLS regression							
Model	**R^2**	**adjust R^2**	**slope**	**intercept**	**slope P-value**	**intercept P-value**	**Formula**
$\log_{10}$(body mass) ~ $\log_{10}$(femur length)	0.943	0.939	2.368	-4.433	5.57E-12	1.26E-11	$\log_{10}$ body mass = 2.368$\log_{10}$X - 4.4327
$\log_{10}$(body mass) ~ $\log_{10}$(femur length add tibia length)	0.937	0.933	2.350	-5.294	1.30E-11	2.46E-11	$\log_{10}$ body mass = 2.3501$\log_{10}$ X - 5.2938
$\log_{10}$(body mass) ~ $\log_{10}$(tibia length)	0.923	0.918	2.319	-4.676	7.10E-11	1.48E-10	$\log_{10}$ body mass = 2.3185$\log_{10}$ X - 4.6758
$\log_{10}$(body mass) ~ $\log_{10}$(humerus length)	0.949	0.946	2.749	-5.128	2.02E-12	3.97E-12	$\log_{10}$ body mass = 2.749$\log_{10}$ X - 5.1282
$\log_{10}$(body mass) ~ $\log_{10}$(humerus length add ulna or radius length)	0.961	0.959	2.775	-6.280	2.05E-13	3.47E-13	$\log_{10}$ body mass = 2.7752$\log_{10}$ X - 6.2801
$\log_{10}$(body mass) ~ $\log_{10}$(ulna or radius length)	0.960	0.958	2.769	-5.647	2.60E-13	4.75E-13	$\log_{10}$ body mass = 2.7694$\log_{10}$ X - 5.6471
$\log_{10}$(body mass) ~ $\log_{10}$(wing metacarpal)	0.883	0.876	1.550	-2.900	2.46E-09	9.34E-09	$\log_{10}$ body mass = 1.5496$\log_{10}$ X - 2.8996

Part2: Bayesian PGLS with CIS tree		
femur		
model	**median R^2**	**marginal liklhood**
random	0.938	-11.9643
delta	0.9489	-12.6673
kappa	0.9454	-12.233
lambda	0.9146	-13.303
ou	0.9425	-12.85
$\log_{10}$ body mass = 2.4476$\log_{10}$ X – 4.5585		
femur and tibia		
model	**median R^2**	**marginal liklhood**
random	0.926723	-13.5807
delta	0.9403	-14.137
kappa	0.9267	-14.1272
lambda	0.904	-14.5271
ou	0.9365	-13.6275
humerus		
model	**median R^2**	**marginal liklhood**

random	0.939249	-11.7735
delta	0.9351	-12.4757
kappa	0.9482	-11.9376
lambda	0.9323	-11.3183
ou	0.949	-11.8112
$\log_{10}$ body mass = 2.4887$\log_{10}$ X – 4.697		
humerus and ulna (radius)		
model	**median R^2**	**marginal liklhood**
random	0.953813	-9.51834
delta	0.9505	-10.287
kappa	0.9554	-9.82147
lambda	0.9446	-9.59502
ou	0.961	-9.0275
$\log_{10}$ body mass = 2.6868$\log_{10}$ X – 6.0288		
tibia		
model	**median R^2**	**marginal liklhood**
random	0.909266	-15.2924
delta	0.9241	-16.1422
kappa	0.9067	-15.8317
lambda	0.8803	-16.1901
ou	0.9225	-15.349
$\log_{10}$ body mass = 2.1635$\log_{10}$ X – 4.363		
ulna		
model	**median R^2**	**marginal liklhood**
random	0.950344	-9.98948
delta	0.9465	-10.6442
kappa	0.9486	-10.4759
lambda	0.9429	-9.65286
ou	0.9599	-9.48722
$\log_{10}$ body mass = 2.8029$\log_{10}$ X – 5.5947		
wing metacarpal		
model	**median R^2**	**marginal liklhood**
random	0.882433	-17.5877
delta	0.8741	-18.1708
kappa	0.892	-17.122
lambda	0.8531	-18.0477
ou	0.8827	-19.4844
$\log_{10}$ body mass = 1.961$\log_{10}$ X – 3.1619		

Table S3. Results of non-phylogenetic OLS regression and Bayesian PGLS regression between $\log_{10}$ transformed limb bone measurements and $\log_{10}$ transformed body mass of the 19 pterosaurs. Relate to Figure 4.

X represents predictor variable.

Part1: Estimated log_{10} body mass for the 101 pterosaurs without body mass data			
species	**Log10 mass**	**species**	**Log10 mass**
Gallodactylus_canjuersensis	0.2979	*Istiodactylus_latidens*	1.338
Alcione_elainus	0.5648	*Istiodactylus_sinensis*	0.7646
Archaeoistiodactylus_linglongtaensis	-0.6155	*Jeholopterus_ningchengensis*	-0.5422
Ardeadactylus_longicollum	-0.0631	*Kunpengopterus_antipollexus*	-0.4542
Aurorazhdarcho_primordius	-0.3273	*Kunpengopterus_sinensis*	-0.8593
Austriadactylus_cristatus	-0.0315	*Kunpengopterus_sp*	-0.5722
Barbosania_gracilirostris	0.7131	*LPM_L112113*	-0.2865
Batrachognathus_volans	-1.2763	*Longchengpterus_zhaoi*	0.2907
Beipiaopterus_chenianus	-0.109	*Maaradactylus_spielbergi*	1.4248
Boreopterus_cuiae	-0.034	*Microtuban_altivolans*	-0.075
Campylognathoides_liasicus	-0.6089	*Mimodactylus_libanensis*	-0.3899
Campylognathoides_zitteli	-0.3293	*Montanazhdarcho_minor*	0.715
Changchengopterus_pani	-0.5458	*Muzquizopteryx_coahuilensis*	0.2397
Chaoyangopterus_zhangi	0.2917	*Nemicolopterus_crypticus*	-1.833
Darwinopterus_linglongtaensis	-0.825	*Nesodactylus_hesperius*	-0.3129
Darwinopterus_modularis	-0.716	*Noripterus_complicidens*	0.1116
Darwinopterus_robustodens	-0.4951	*Noripterus_parvus*	0.2484
Dendrorhynchoides_curvidentatus	-1.5127	*Nyctosaurus_grandis*	1.4158
Dendrorhynchoides_mutoudengensis	-1.3921	*Painten_pterodactyloid*	-1.0281
Dimorphodon_weintraubi	0.2712	*Peteinosaurus_zambelli*	-0.784
Dorygnathus_banthensis	0.1532	*Pteranodon_sternbergi*	0.977
Douzhanopterus_zhengi	-0.7216	*Pterodactylus_kochi*	-0.8705
Elanodactylus_prolatus	0.5762	*Pterodactylus_micronyx*	-1.4368
Eoazhdarcho_liaoxiensis	0.265	*Pterorhynchus_wellnhoferi*	-0.3896
Eopteranodon_lii	-0.0492	*Raeticodactylus_filisurensis*	0.1121
Eosipterus_yangi	-0.0361	*Rhamphorhynchus_etchesi*	0.0209
Eudimorphodon_rosenfeldi	-1.1506	*Scaphognathus_crassirostris*	-0.2462
Fenghuangopterus_lii	-0.2611	*Seazzadactylus_venieri*	-0.6404
Gegepterus_changae	-0.5143	*Shenzhoupterus_chaoyangensis*	7.88E-03
Germanodactylus_cristatus	-0.4466	*Sinomacrops_bondei*	-1.5581
Germanodactylus_rhamphastinus	-0.4684	*Sinopterus_gui*	-0.7173
Haopterus_gracilis	-0.1116	*Tapejara_wellnhoferi*	0.1552
Huaxiapterus_benxiensis	0.0306	*Tropeognathus_mesembrinus*	1.8481
Huaxiapterus_jii	0.2015	*Tupuxuara_leonardii*	1.3036
Ikrandraco_avatar	0.0597	*Versperopterylus_lamadongensis*	-0.4611
Wukongopterus_lii	-0.7747	*Nyctosaurus_nanus*	0.219
Wukongopterus_sp	-0.7124	*Radiodactylus_langstoni*	1.2734
Zhenyuanopterus_longiristris	1.0314	*Sericipterus_wucaiwanensis*	0.3793
Alamodactylus_byrdi	1.0395	*Simurghia_robusta*	1.2161
Anhanguera_araripensis	1.0378	*Gladocephaloideus_jingangshanensis*	-0.3248

Anhanguera_robustus	1.217	*Anhanguera_santanae*	0.9541
Austriadraco_dallavecchiai	-0.6644	*Arambourgiania_philadelphiae*	2.2895
Azhdarcho_lancicollis	0.9278	*Ferrodraco_lentoni*	0.9925
Bennettazhia_oregonensis	1.0244	*Hamipterus_tianshanensis*	0.8602
Caiuajara_dobruskii	0.232	*Jianchangnathus_robustus*	0.0693
Caupedactylus_ybaka	0.9713	*Keresdrakon_vilsoni*	0.9338
Hatzegopteryx_thambena	2.2963	*Piksi_barbarulna*	-0.199
Kepodactylus_insperatus	0.52	*Tethydraco_regalis*	1.6248
Kryptodrakon_progenitor	-0.0307	*Yixianopterus_jingangshanensis*	0.3947
Nyctosaurus_bonneri	0.742	*Eurazhdarcho_langendorfensis*	0.726
Nyctosaurus_lamegoi	1.2496		
Part2: Log 10 transformed body mass data for the 19 pterosaurs in Witton 2008			
species	**Log10 mass**	**species**	**Log10 mass**
Preondactylus_buffarinii	-1.09691	*Pterodactylus_antiquus*	-1.0172
Dimorphodon_macronyx	-0.0118	*Ctenochasma_elegans*	-0.8004
Eudimorphodon_ranzii	-0.5956	*Pterodaustro_guinazui*	-0.0352
Rhamphorhynchus_muensteri	-0.886	*Huanhepterus_quingyangensis*	0.764923
Sordes_pilosus	-0.85387	*Dsungaripterus_weii*	0.954725
Anurognathus_ammoni	-1.39794	*Sinopterus_dongi*	-0.279
Nurhachius_ignaciobritoi	0.60206	*Huaxiapterus_corallatus*	0.012837
Anhanguera_piscator	1.078457	*Zhejiangopterus_linhaiensis*	1.0265
Pteranodon_longiceps	1.694	*Quetzalcoatlus_northropi*	2.3196
Nyctosaurus_gracilis	-0.0168		

Part3: Marginal likelihood of body mass evolutionary rate models			
Part1+Part2		**Part1 + log transformed body mass taken from Witton 2008**	
Using all taxa		**Using all taxa**	
model	**marginal likelihood**	**model**	**marginal likelihood**
single rate BM	-186.130	single rate BM	-146.124
BM	-131.930	BM	-130.170
lambda	-124.107	lambda	-122.548
kappa	-126.305	kappa	-122.0397
delta	-135.862	delta	-130.879
Without *Nemicolopterus crypticus*		**Without *Nemicolopterus crypticus***	
model	**marginal likelihood**	**model**	**marginal likelihood**
single rate BM	-184.0539	single rate BM	-141.691
BM	-131.0619	BM	-126.466
kappa	-120.767	kappa	-116.121
lambda	-120.617	lambda	-117.364
delta	-130.318	delta	-125.930

Table S4. Estimated log_{10} body mass body mass and body mass evolutionary rate model selection. Relate to Figure 4.

In part2, boxes in orange means that the species has multiple specimens and the body mass were re-estimated with the Bayesian PGLS model, and in light blue means that the data was log transformed from the original data in Witton 2008 [S48].

Supplemental References

S1. Vidovic, S.U., and Martill, D.M. (2017). The taxonomy and phylogeny of Diopecephalus kochi (Wagner, 1837) and ' Germanodactylus rhamphastinus ' (Wagner, 1851). Geological Society London Special Publications *455*, SP455.412.

S2. Kellner, A., Caldwell, M.W., Holgado, B., Vecchia, F.M.D., Nohra, R., Sayo, J.M., and Currie, P.J. (2019). First complete pterosaur from the Afro-Arabian continent: insight into pterodactyloid diversity. Sci. Rep. *9*.

S3. Jacobs, M.L., Martill, D.M., Ibrahim, N., and Longrich, N. (2018). A new species of Coloborhynchus (Pterosauria, Ornithocheiridae) from the mid-Cretaceous of North Africa. Cretac. Res. *95*.

S4. Martill, D.M., Smith, R., Unwin, D.M., Kao, A., McPhee, J., and Ibrahim, N. (2020). A new tapejarid (Pterosauria, Azhdarchoidea) from the mid-Cretaceous Kem Kem beds of Takmout, southern Morocco. Cretac. Res. *112*, 104424.

S5. Pentland, A.H., Poropat, S.F., Tischler, T.R., Sloan, T., Elliott, R.A., Elliott, H.A., Elliott, J.A., and Elliott, D.A. (2019). *Ferrodraco lentoni* gen. et sp. nov., a new ornithocheirid pterosaur from the Winton Formation (Cenomanian–lower Turonian) of Queensland, Australia. Sci. Rep. *9*, 13454.

S6. Wu, W.H., Zhou, C.F., Brian, A., and Matt, F. (2017). The toothless pterosaur Jidapterus edentus (Pterodactyloidea: Azhdarchoidea) from the Early Cretaceous Jehol Biota and its paleoecological implications. PLoS ONE *12*, e0185486.

S7. Pêgas, R.V., Holgado, B., and Leal, M.E.C. (2021). On Targaryendraco wiedenrothi gen. nov. (Pterodactyloidea, Pteranodontoidea, Lanceodontia) and recognition of a new cosmopolitan lineage of Cretaceous toothed pterodactyloids. Historical Biology *33*, 1266-1280.

S8. Rodrigues, T., and Kellner, A.W.A. (2013). Taxonomic review of the Ornithocheirus complex (Pterosauria) from the Cretaceous of England. ZooKeys *308*, 1–112.

S9. Pinheiro, F.L., Fortier, D.C., Schultz, C.L., Andrade, J.D., and Bantim, R. (2011). New information on the pterosaur Tupandactylus imperator, with comments on the relationships of Tapejaridae. Acta Palaeontol. Pol. *56*, 567-580.

S10. Headden, J.A., and Campos, H.B.N. (2015). An unusual edentulous pterosaur from the Early Cretaceous Romualdo Formation of Brazil. Historical Biology *27*, 815-826.

S11. Hone, D., Fitch, A., Ma, F., and Xu, X. (2020). An unusual new genus of istiodactylid pterosaurfrom China based on a near complete specimen. Palaeontologia Electronica *23*.

S12. Pêgas, R.V., Leal, M.E.D.C., and Kellner, A.W.A. (2016). A Basal Tapejarine (Pterosauria; Pterodactyloidea; Tapejaridae) from the Crato Formation, Early Cretaceous of Brazil. PLoS ONE *11*, e0162692.

S13. Holgado, B., Pêgas, R.V., Canudo, J.I., Fortuny, J., Rodrigues, T., Company, J., and Kellner, A. (2019). On a new crested pterodactyloid from the Early Cretaceous of the Iberian Peninsula and the radiation of the clade Anhangueria. Sci. Rep. *9*, 4940.

S14. Maisch, M.W., Matzke, A.T., and Ge, S. (2004). A new dsungaripteroid pterosaur from the Lower Cretaceous of the southern Junggar Basin, north-west China. Cretac. Res. *25*, 625-634.

S15. Andres, B., Clark, J., and Xu, X. (2014). The Earliest Pterodactyloid and the Origin of the Group. Curr. Biol. *24*, 1011-1016.
S16. Junchang, L., Martin, K., Shen, C., and Anthony, F. (2016). New Material of the Pterosaur Gladocephaloideus Lü et al., 2012 from the Early Cretaceous of Liaoning Province, China, with Comments on Its Systematic Position. PLoS ONE *11*, e0154888.
S17. Wei, X., Pêgas, R.V., Shen, C., Guo, Y., and Zhou, X. (2021). Sinomacrops bondei , a new anurognathid pterosaur from the Jurassic of China and comments on the group. Peer J *9*, e11161.
S18. Bantim, R.A.M., Saraiva, A.A.F., Oliveira, G.R., and Sayao, J.M. (2014). A new toothed pterosaur (Pterodactyloidea: Anhangueridae) from the Early Cretaceous Romualdo Formation, NE Brazil. Zootaxa *3869*, 201-223.
S19. Zhou, X., Pêgas, R.V., Leal, M.E.C., and Bonde, N. (2019). Nurhachius luei, a new istiodactylid pterosaur (Pterosauria, Pterodactyloidea) from the Early Cretaceous Jiufotang Formation of Chaoyang City, Liaoning Province (China) and comments on the Istiodactylidae. Peer J *7*, e7688.
S20. J, S.-X., Z, X.-J., C, X., and W, X. (2021). A new pteranodontoid pterosaur forelimb from the upper Yixian Formation, with a revision of Yixianopterus jingangshanensis. Vertebrata PalAsiatica *1000-3118*, 201124.
S21. Zhou, C.F., Gao, K.Q., Yi, H., Xue, J., Li, Q., and Fox, R.C. (2017). Earliest filter-feeding pterosaur from the Jurassic of China and ecological evolution of Pterodactyloidea. R. Soc. Open Sci. *4*, 160672.
S22. Jiang, S.X., Wang, X.L., Meng, X., and Cheng, X. (2014). A new boreopterid pterosaur from the Lower Cretaceous of western Liaoning, China, with a reassessment of the phylogenetic relationships of the Boreopteridae. Journal of Paleontology *88*, 823-828.
S23. Codorniú, L., Paulina-Carabajal, A., Pol, D., Unwin, D., and Rauhut, O.W. (2016). A Jurassic pterosaur from Patagonia and the origin of the pterodactyloid neurocranium. Peer J *4*, e2311.
S24. Junchang, L., and HONE, D.W.E. (2012). A New Chinese Anurognathid Pterosaur and the Evolution of Pterosaurian Tail Lengths. Acta Geologica Sinica *86*, 1317-1325.
S25. Bennett, S.C. (2007). A second specimen of the pterosaur Anurognathus ammoni. Paläontologische Zeitschrift *81*, 376-398.
S26. Kellner, A.W., Campos, D.A., Sayão, J.M., Saraiva, A.A., Rodrigues, T., Oliveira, G., Cruz, L.A., Costa, F.R., Silva, H.P., and Ferreira, J.S. (2013). The largest flying reptile from Gondwana: a new specimen of Tropeognathus cf. T. mesembrinus Wellnhofer, 1987 (Pterodactyloidea, Anhangueridae) and other large pterosaurs from the Romualdo Formation, Lower Cretaceous, Brazil. An Acad Bras Cienc *85*, 113-135.
S27. Longrich, N.R., Martill, D.M., and Andres, B. (2018). Late Maastrichtian pterosaurs from North Africa and mass extinction of Pterosauria at the Cretaceous-Paleogene boundary. PLoS Biol. *16*, e2001663.
S28. Clark, J.M., Hopson, J.A., Hernández R, R., Fastovsky, D.E., and Montellano, M. (1998). Foot posture in a primitive pterosaur. Nature *391*, 886-889.
S29. Lü, J.C., Fucha, X.H., and Chen, J.M. (2010). A New Scaphognathine Pterosaur from the Middle Jurassic of Western Liaoning,China. Acta Geoentica Sinica *31*, 263-266.
S30. Buffetaut, E., Grigorescu, D., and Csiki, Z. (2002). A new giant pterosaur with a robust

skull from the latest Cretaceous of Romania. Naturwissenschaften *89*, 180-184.

S31. Marsh, O.C. (1881). Note on American pterodactyls. American Journal of Science *s3-21*, 342-343.

S32. Dalla Vecchia, F.M. (2019). Seazzadactylus venieri gen. et sp. nov., a new pterosaur (Diapsida: Pterosauria) from the Upper Triassic (Norian) of northeastern Italy. Peer J *7*, e7363.

S33. O'Sullivan, M., and Martill, D.M. (2018). Pterosauria of the Great Oolite Group (Bathonian, Middle Jurassic) of Oxfordshire and Gloucestershire, England. Acta Palaeontol. Pol. *63(4)*, 617–644.

S34. Cheng, X., Jiang, S., Wang, X., and Kellner, A.W. (2016). New information on the Wukongopteridae (Pterosauria) revealed by a new specimen from the Jurassic of China. Peer J *4*, e2177.

S35. Zhou, X., Pêgas, R.V., Ma, W., Han, G., Jin, X., Leal, M.E.C., Bonde, N., Kobayashi, Y., Lautenschlager, S., Wei, X., et al. (2021). A new darwinopteran pterosaur reveals arborealism and an opposed thumb. Curr. Biol. *31*, 2429-2436.e2427.

S36. Lü, J., Unwin, D.M., Deeming, D.C., Jin, X., Liu, Y., and Ji, Q. (2011). An egg-adult association, gender, and reproduction in pterosaurs. Science *331*, 321-324.

S37. Eberhard.Frey, and Helmut.Tischlinger (2013). A new pterosaur with mosaic characters of basal and pterodactyloid pterosauria from the Upper Kimmeridgian of Painten (Upper Palatinate, Germany). Archaeopteryx *31*, 1-13.

S38. Vidovic, S.U., and Martill, D.M. (2014). Pterodactylus scolopaciceps Meyer, 1860 (Pterosauria, Pterodactyloidea) from the Upper Jurassic of Bavaria, Germany: The Problem of Cryptic Pterosaur Taxa in Early Ontogeny. PLoS ONE *9*, 1-16.

S39. Naish, D., Simpson, M., and Dyke, G. (2013). A New Small-Bodied Azhdarchoid Pterosaur from the Lower Cretaceous of England and Its Implications for Pterosaur Anatomy, Diversity and Phylogeny. PLoS ONE *8*, e58451.

S40. Jiang, S., and Wang, X. (2011). A new ctenochasmatid pterosaur from the Lower Cretaceous, western Liaoning, China. An Acad Bras Cienc *83*, 1243-1249.

S41. Rodrigues, T., Jiang, S., Cheng, X., Wang, X., and Kellner, A.W.A. (2015). A new toothed pteranodontoid (Pterosauria, Pterodactyloidea) from the Jiufotang Formation (Lower Cretaceous, Aptian) of China and comments on Liaoningopterus gui Wang and Zhou, 2003. Historical Biology *27*, 782-795.

S42. Wang, X., Kellner, A.W.A., Jiang, S., Wang, Q., Ma, Y., Paidoula, Y., Cheng, X., Rodrigues, T., Meng, X., Zhang, J., et al. (2014). Sexually dimorphic tridimensionally preserved pterosaurs and their eggs from China. Curr. Biol. *24*, 1323-1330.

S43. Lü, J., Meng, Q., Wang, B., Liu, D., Shen, C., and Zhang, Y. (2017). Short note on a new anurognathid pterosaur with evidence of perching behaviour from Jianchang of Liaoning Province, China. Geological Society London Special Publications, SP455.416.

S44. Vecchia, F. (1993). Cearadactylus? ligabuei, nov. sp., a new Early Cretaceous (Aptian) pterosaur from Chapada do Araripe (Northeastern Brazil). Boll. Soc. Paleontol. Ital. *32*, 401-409.

S45. Kellner, A.W.A., Rodrigues, T., and Costa, F.R. (2011). Short note on a Pteranodontoid pterosaur (Pterodactyloidea) from western Queensland, Australia. An Acad Bras Cienc *83*, 301-308.

S46. Myers, T.S. (2015). First North American occurrence of the toothed pteranodontoid pterosaur Cimoliopterus. J. Vertebr. Paleontol. *35*, e1014904.
S47. Varricchio, D.J. (2002). A new bird from the Upper Cretaceous Two Medicine Formation of Montana. Canadian Journal of Earth Sciences *39*, 19-26.
S48. Witton, M.P. (2008). A new approach to determining pterosaur body mass and its implications for pterosaur flight. Zitteliana Reihe B: Abhandlungen der Bayerischen Staatssammlung fur Palaontologie und Geologie *B28*, 143-158.